DEVELOPMENT OF A KINEMATIC FOREARM MODEL WITH MOVING ROTATION AXIS FOR PRO/SUPINATION MOTION

A THESIS SUBMITTED TO
THE BOARD OF GRADUATE PROGRAMS
OF
MIDDLE EAST TECHNICAL UNIVERSITY, NORTHERN CYPRUS CAMPUS

BY

MATTHEW ARAZ

IN PARTIAL FULFILLMENT OF THE REQUIREMENTS
FOR
THE DEGREE OF MASTER OF SCIENCE
IN MECHANICAL ENGINEERING PROGRAM

AUGUST 2021

Approval of the Board of Graduate Programs

Prof. Dr. Oğuz Solyalı

Chairperson

I certify that this thesis satisfies all the requirements as a thesis for the degree of Master of Science

Prof. Dr. Eşref Eşkinat

Program Coordinator

This is to certify that we have read this thesis and that in our opinion it is fully adequate, in scope and quality, as a thesis for the degree of Master of Science.

Dr. Behzat Bahadır Kentel	Assoc. Prof. Dr. Volkan Esat
Co-Supervisor	Supervisor

Examining Committee Members

Prof. Dr. Eşref Eşkinat	METU NCC / MECH	
Assoc. Prof. Dr. Volkan Esat	METU NCC / MECH	
Dr. Behzat Bahadır Kentel	Atılım University/ Mechanical Engineering	
Asst. Prof. Dr. Anna Prach	METU NCC / ASE	
Asst. Prof. Dr. Bülent İrfanoğlu	Atılım University / Mechatronics Engineering	

I hereby declare that all information in this document has been obtained and presented in accordance with academic rules and ethical conduct. I also declare that, as required by these rules and conduct, I have fully cited and referenced all material and results that are not original to this work.

Name, Last name : Matthew Araz

Signature :

ABSTRACT

DEVELOPMENT OF A KINEMATIC FOREARM MODEL WITH MOVING ROTATION AXIS FOR PRO/SUPINATION MOTION

Araz, Matthew
Master of Science, Mechanical Engineering Program
Supervisor: Assoc. Prof. Dr. Volkan Esat
Co-Supervisor: Dr. Behzat Bahadır Kental

August 2021, 81 pages

Understanding the biomechanics of the forearm motion is essential for many research areas to improve the quality of human life. In this study, a new kinematic forearm model is proposed for estimating the rotation axis and obtaining proper forearm orientation during the pro/supination motion. As an improvement, a moving rotation axis is included as a link inside the model, and the rotation of the radius segment around the moving rotation axis is investigated. The model is tested in different motion patterns and compared with the rotation around tilted fixed axis as well as the experimental motion data. The outcome of the model shows that with defining the pro/supination motion as a rotation around the moving rotation axis (MRA), the trajectories and the range of motions of the radius are obtained within the expected ranges according to the literature. Besides, the MRA model provides more reliable results compared with the fixed axis. The comparison with the experimental analysis shows that the radius trajectory of the model is compatible with the motion data. For further investigations, with the subject specific adjustment, the proposed model can provide better understanding on the forearm kinematics.

Keywords: Forearm biomechanics, Pro/supination motion, Moving rotation axis, Kinematic modelling

ÖZ

PRONASYON / SÜPİNASYON HAREKETİ İÇİN SABİT OLMAYAN BİR DÖNME EKSENİ İÇEREN KİNEMATİK ÖN KOL MODELİNİN GELİŞTİRİLMESİ

Araz, Matthew
Yüksek Lisans, Makina Mühendisliği
Tez Yöneticisi: Doç. Dr. Volkan Esat
Ortak Tez Yöneticisi: Dr. Behzat Bahadır Kentel

Ağustos 2021, 81 sayfa

Önkol hareketinin biyomekaniğini anlamak, insan yaşam kalitesini iyileştirmek için birçok araştırma alanında büyük önem taşımaktadır. Bu çalışmada, pro/supinasyon hareketi sırasında rotasyon ekseninin yerini kestirmek ve uygun önkol oryantasyonunu elde etmek için yeni bir kinematik önkol modeli önerilmiştir. Önceki çalışmalardan farklı olarak, dönme ekseni modelin uzuvlarından biri olarak tanımlanmış ve önkol (radius) kemiğinin hareketli dönme ekseni etrafındaki dönüşü incelenmiştir. Model, hareketli eksen kayması için tanımlanmış yuva ekleminin farklı konumlarında test edilmiş ve deneysel hareket verisi ve sabit eksenli model ile karşılaştırılmıştır. Pro/supinasyon hareketi, hareketli dönme ekseni (MRA) etrafında tanımlandığında, önkol kemiğinin yörüngesi ve hareket aralığı için elde edilen sonuçlar literatüre göre beklenen aralıklar içerisinde elde edilmiştir. Ayrıca MRA modelinin sabit eksene göre daha güvenilir sonuçlar verdiği gözlemlenmiştir. Deneysel analizle kıyaslama sonucunda modeldeki önkol kemiği yörüngesinin hareket verileriyle uyumlu hareket ettiği görülmüştür. İlerideki çalışmalar için, modelin kişiye özel ayarlanmasıyla önkol kinematiği üzerinde daha gerçekçi bir anlayış sağlayabileceği öngörülmektedir.

Anahtar Kelimeler: Ön kol biyomekaniği, Pro/supinasyon hareketi, Hareketli dönme ekseni, Kinematik modelleme

To ones who always love and support me…

ACKNOWLEDGEMENTS

I would like to express my deepest gratitude to my advisors Dr. Behzat Bahadır Kentel and Assoc. Prof. Dr. Volkan Esat for their guidance, endless support, patience, and encouragement throughout my academic life. They have been amazing mentors and truly inspiring professors for me.

Besides my advisors, I also would like to thank the current and past faculty members of the Mechanical Engineering department: Prof. Dr. Eşref Eşkinat, Asst. Prof. Dr. Ali Berk Başta̧ş, Assoc. Prof. Dr. Onur Taylan, Assoc. Prof. Dr. Eray Uzgören, Asst. Prof. Dr. Ali Atashbar Orang and Assoc. Prof. Dr. Murat Sönmez. They have always been supportive and helpful without a hesitation.

I also would like to thank the jury members Asst. Prof. Dr. Anna Prach and Asst. Prof. Dr. Bülent İrfanoğlu for their time and valuable comments on thesis.

I am extremely grateful to my family for their endless love and support throughout my life. My father Kerim Araz, my mother Firyal Kahraman and my older brother Jack Araz have always been supported my decisions, and they always encouraged me to push myself to reach the success. They always believed in me without hesitation.

After the 9-year journey, METU NCC becomes my second home. I would like to thank my friends for our amazing memories that I will never forget. I also would like to appreciate Nilay Gençer for her constant support and encouragement in the last 2 years of my life.

Lastly but not least, I want to thank our campus dogs and cats; Abbath, Karamel, Süslü, Latte, Flake, Hedwig, Victor, Şahika and many others for making the pandemic period more fun and joyful for us. During the pandemic, we had rough times, but their pure emotions and funny actions made our days more enjoyable.

This work is supported by Middle East Technical University Northern Cyprus Campus, Grant. Number: BAPFEN-18-D9.

TABLE OF CONTENTS

LIST OF TABLES

TABLES

LIST OF FIGURES

FIGURES

LIST OF ABBREVIATIONS

ABBREVIATIONS	
CT	Computed Tomography
D	Distal
DOF	Degree of Freedom
DRH	Distal Radius Head
DRUJ	Distal Radioulnar Joint
DUH	Distal Ulna Head
FE	Flexion/Extension
FRA	Fixed Rotation Axis
HR	Humeroradial
HU	Humeroulnar
IOM	Interosseous Membrane
LED	Light-emitting diode
MRA	Moving Rotation Axis
MRI	Magnetic Resonance Imaging
MRUJ	Middle Radioulnar Joint
P	Proximal
PRH	Proximal Radius Head
PRUJ	Proximal Radioulnar Joint
PUH	Proximal Ulna Head
PS	Pro/Supination

R	Radius
REJC	Right Elbow Joint Centre
ROM	Range of Motion
RSJC	Right Shoulder Joint Centre
RWJC	Right Wrist Joint Centre
TFCC	Triangular Fibrocartilage Complex Cartilage
U	Ulna
UMRA	Ulna-MRA Joint (Slot that MRA translates inside)

LIST OF SYMBOLS

SYMBOLS	
f	Joint Degree of Freedom
j	Number of joints
l	Number of links
r_1	Elbow
r_2	Ulna
r_3	Offset
r_4	MRA
r_5	Radius
s_1	Axial Ulna Translation
s_2	Orientation of MRA at the Distal Ulna Head
γ	Inclination of the MRA slot
θ	Pro/supination Angle
λ	Degree of Freedom in Space
ϕ_1	Rotation of MRA along the z axis
ϕ_2	Rotation of MRA along the x axis

CHAPTER 1

INTRODUCTION

1.1 Motivation

In our daily life, every human being needs to have upper extremity functionality to be able perform many daily routine activities such as transferring a glass or food from table to mouth to drink water or eat that food, reaching to an object which is away from us, carrying a box, grasping bag and transferring it somewhere else, etc. Even though performing these tasks looks like extremely basic and easy, most of them involve complex mechanics. The upper limb of a human body consists of 4 different segments which are shoulder, arm, forearm and hand, with joints between each segment. Among these 4 segments, the forearm segment has a special motion about which is called pro/supination (PS) motion. This special motion, which is the longitudinal rotation of forearm, is observed on the animals whose ancestors were arboreal animals over million years ago (Soubeyrand et al., 2017). Since they were an animal type who lives on the tree, they were grasping branches of the trees to change their locations from one tree to another. Evolution theory pointed out that, our ancestors started to perform bipedal gait, their forelimbs turned into the upper limbs, and they used these limbs to get interaction with the environment and their body. To survive in the wildlife, they needed to use their upper limbs for more precise tasks, thus the bone and joint structures of the hand and the forearm evolved to be able to perform wrist manipulation and forearm pro/supination. As a result of the evolutionary progress, the forearm and wrist biomechanics reached to their current functionality.

The forearm performs pro/supination motion and works as a load transfer unit between hand and arm. These two biomechanical functionalities of the forearm have

essential contributions to many daily activities, and having a better understanding of the forearm physiology and biomechanics is crucial for many research areas such as medical, sports, robotic and prosthetics, etc. As a result, doctors and physiotherapists can improve surgeries and rehabilitation treatments, new medical devices can be designed according to the biomechanics of forearm, coaches can improve the techniques of the exercises so that athletes can use their potential at the maximum level and prevent them from the injuries, human-robot interactions can be brought to a new level so that humanoid robots can mimic the human motion properly and they can be used in dangerous working areas, or new prosthetic systems can be developed to improve life quality of the disabled people.

From the late 19th century, researchers have been working on the biomechanics of the forearm motion. These studies have been investigating the forearm motion from different aspects to be able to understand the kinematics of the bones and joints. Some of these studies analysed the motion by conducting in vitro and in vivo motion experiments, and some of them tried to simulate the motion with building kinematic models to explain the mechanics of it. Even though the motion analysis gives valid understanding on the motion, the small gliding motions of soft tissues on the bones might mislead the researchers about the bone motions. Thus, kinematic models play a significant role on the defining the normal and abnormal bone motions (Robbin et al., 1986).

Understanding the proper musculoskeletal kinematics and building kinematic models to simulate the motion have been helping many fields to improve their research, techniques, and devices. In the medical field, new surgery and rehabilitation devices have been built according to motion expressions of the kinematic models, and the treatment strategies in rehabilitation has been improved over the years (Guo et al., 2013; Nojiri et al., 2006). Kinematic models pave the way for the development of exoskeletal rehabilitation robots, thus the efficacy of the rehabilitation treatments are improved with the use of new technologies in the treatment process (Guo et al., 2013). In addition to the surgery and rehabilitation

devices, the prosthetic designs are also remodelled with better kinematics knowledge. The ergonomics of disabled people is extremely critical on the prosthetic designs since the prosthetic might create unwanted stresses on the bones. To prevent bones from the potentially possible stresses, the outcomes of the kinematic models plays an important role on the prosthetics design (Robbin et al., 1986). Not only the medical devices but also the daily life products are designed according to the outcomes obtained from kinematic models of the musculoskeletal systems. Since human performance, safety and ergonomics are the essential consideration factors, limb models are used to test the products in virtual environments to improve the human-machine interactions (Pennestrì et al., 2007).

Due to the complex physiology of the forearm, modelling and analysing the kinematics of the forearm is still a challenging task and requires more investigations. With more realistic modelling of the forearm, the knowledge of the complex forearm biomechanics can be improved, and it may lead the further improvements on many medical devices, surgery and treatment techniques, and the ergonomics and safety considerations on many products that we use in our daily life routines.

1.2 Objective of Thesis

The main objective of this thesis is to develop a new kinematic forearm model which estimates the PS axis of the forearm. In this study, a realistic two-segment (radius-ulna), novel, closed-loop forearm model is proposed to simulate the PS motion of the forearm. The proposed model includes the rotation axis as one of the links of the model, and the model allows the translation and rotation motions of the rotation axis to simulate the anatomical PS axis of human forearm. In the literature, some of the studies defined a fixed rotation axis for PS motion (Hagert, 1992; Hollister et al., 1994b; Oka et al., 2006; Ray et al., 1951; Youm et al., 1979), however more recent studies showed that the location of axis is changing during the PS motion (Nakamura et al., 1999; Tay et al., 2008, 2010; Veeger et al., 1996). In this study, the rotation

axis motion is designed according to the findings of Tay et al. (2008, 2010). The rotation axis of the model is designed as a moving link, and it is named as the moving rotation axis (MRA). The PS motion is defined on the MRA unlike the previous kinematic models. Since the model directly rotates around the actual rotation axis, it is expected to observe a consistent radius trajectory within an acceptable range of motion for the radius rotation compared with the literature and the experimental motion data. In addition, a fixed rotation axis and an MRA for PS motion will be compared to determine the role of MRA in forearm motion.

1.3 Outline of the Thesis

The following chapters of the thesis explain the conducted work in detail. The thesis contains 7 chapters, and the rest of the thesis continues as follows;

In Chapter 2, a detailed literature review is provided and includes 3 sections. In the first section, the anatomy and biomechanics of the forearm is explained. In the second section, how previous motion analysis studies located rotation axis on the forearm is discussed. Finally, in the third section, the mechanical structures of the previous kinematic models are explained in detail.

In Chapter 3, the proposed model is discussed. The mechanical structure of the model, and how radioulnar joint is mechanically modelled is presented.

In Chapter 4, the kinematics analysis applied on the model is explained. How inverse and forward kinematics are used in the position analysis of the model is presented with the analytical solutions.

In Chapter 5, the analysis conducted on the motion data is explained. First, the task in the experimentation and the marker set is explained. Then, methodology of the locating joint centres and defining local frames of the segments are described, and finally the procedure in kinematic analysis is provided.

In Chapter 6, the results obtained from the proposed model is discussed with the findings of the previous studies. The radius trajectory obtained from the model is compared with the radius trajectory that is obtained from the experimental data for the validation of the model. In addition, the comparison between fixed axis and moving axis is presented.

In Chapter 7, the conclusion is presented with possible future work.

CHAPTER 2

LITERATURE REVIEW

2.1 Anatomy & Biomechanics of Forearm

Upper extremity is the portion of human body which consists of the shoulder, arm, elbow, forearm, wrist, and hand as shown in Figure 2.1 (a). The forearm (Figure 2.1) unit is a complex structure which exists as a connector between the arm and hand. It plays a significant role in load transmission between the hand and the arm, and in the hand orientation in space during the upper extremity motion (Dumontier & Soubeyrand, 2013). The forearm is connected to the upper arm via elbow at its proximal end and to the hand via wrist at its distal end. Between these two joints, the forearm comprises of the two bones radius and ulna, three complex radioulnar joints, the ligaments that bond these two bones to each other, and the muscles which are responsible from the forearm and the hand rotation, and the motion of the fingers. The forearm unit has two degree of freedom (DOF) which are flexion/extension (FE) and pronation/supination (PS) motions of the forearm. The FE motion is the rotation of forearm about an instantaneous axes which passes from the sagittal plane of the elbow (Morrey et al., 2018; Zimmerman, 2002). On the other hand, the PS motion is the longitudinal rotation of the forearm resulting in the palm up and down orientations of the hand (Kapandji, 2007; Soubeyrand et al., 2017). Figure 2.2 shows the palm orientations according to the pronation and supination poses. The palm looks upward in the maximum supination pose and downwards at the maximum pronation pose. In PS motion where the thumb looks upward is called the neutral pose of the forearm which is the reference point to define ranges of both pronation and supination separately (Kapandji, 2007).

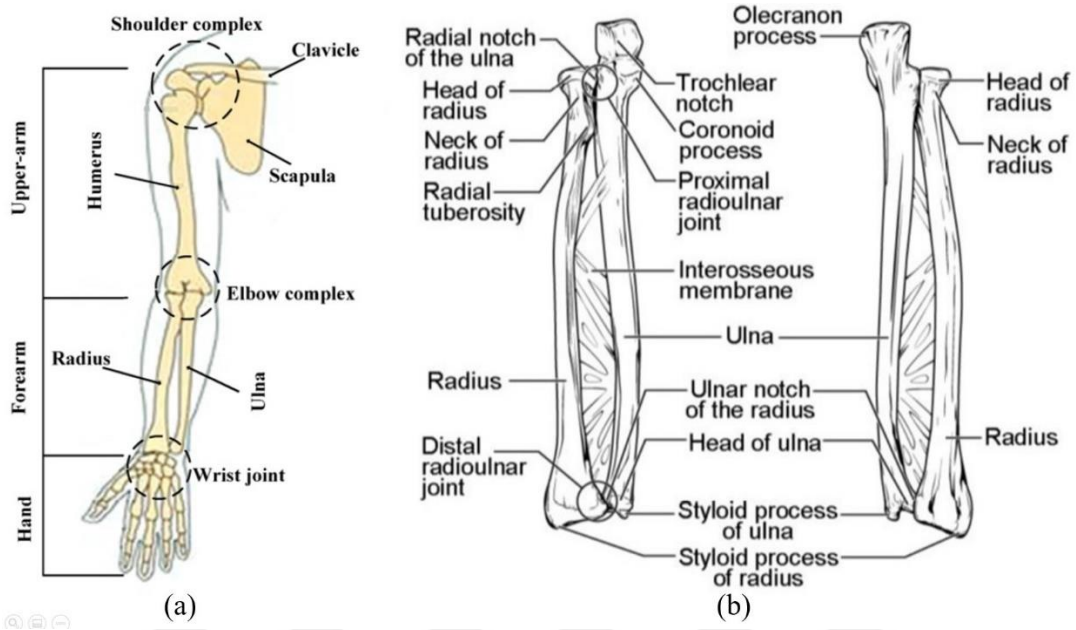

Figure 2.1 (a) Upper limb of the human body (Chen et al., 2014) (b)Anatomy of the complex forearm unit

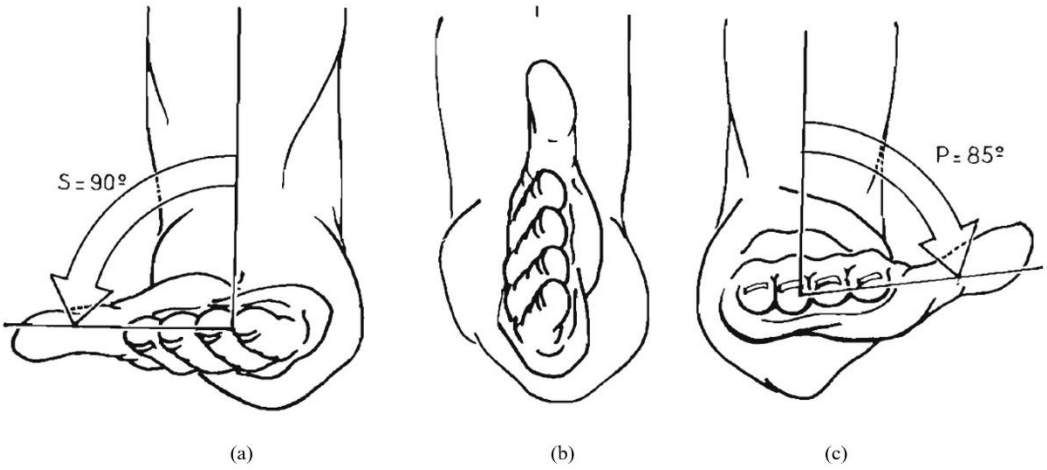

Figure 2.2 (a) Maximum Supination, (b) neutral, and (c) maximum pronation poses of the forearm (Kapandji, 2007)

The forearm bones radius and ulna are curved shaped bones which has asymmetrical epiphyses. As shown in Figure 2.1, the ulnar epiphysis at the proximal end and the radial epiphysis at the distal end is bigger than the size of adjacent bone's head. Due to the asymmetrical shapes of the bones, the centres of bone heads are not located

aligned with each other. This difference is called as radioulnar variance, and it exists at both proximal and distal ends of forearm. The ulna head has proximal offset at the proximal side, and the radius has distal offset at the distal side (Soubeyrand et al., 2017). These offsets are the connection points of the ulna and the radius with the humerus and the carpus, respectively. At the elbow side, the articulation of the trochlear notch of the ulna (greater sigmoid notch) and the trochlea of humerus forms the hinge structured humeroulnar joint which allows the flexion/extension (FE) motion of the forearm. In addition, the fovea radialis is also in contact with capitellum of the humerus which is a trochoid type of joint called humeroradial (HR) or radiocapitellar joint allows pronation/supination (PS) motion of the forearm with radioulnar joint (Alcid et al., 2004; Doyle & Botte, 2003). At the wrist side, the radius head articulates with scaphoid and lunate bones of carpus which forms the radiocarpal (RC) joint (Doyle & Botte, 2003). This joint allows the FE and radioulnar deviation of the hand unit (Palmer et al., 1985).

2.1.1 Radioulnar Joint

The forearm unit can be divided into three parts as proximal, middle, and distal sections as shown in Figure 2.1. At the proximal and distal ends of the forearm, the radius and ulna bones are connected to each other with the proximal radioulnar (PRUJ) and distal radioulnar (DRUJ) joints. Middle section is the section between the PRUJ and DRUJ, and at this section, there is a gap between the radius and the ulna which is filled by multicomponent ligamentous structure called interosseous membrane (IOM). The IOM links radius and ulna shafts from one end to the other end between the PRUJ and DRUJ. Thus, this connection between the bone shafts is called as middle radioulnar joint (MRUJ) (Dumontier & Soubeyrand, 2013; LaStayo & Lee, 2006; Soubeyrand et al., 2017). These three joints are not independently functional. They contribute to the PS motion together, and any damage occurred at one of them affects the rotation capability of the forearm. Since the whole forearm

unit is the combination of the radioulnar joints, the unit can be called as forearm joint to get better understanding on its physiology (Dumontier & Soubeyrand, 2013).

2.1.1.1 Proximal Radioulnar Joint (PRUJ)

The PRUJ is the joint where proximal radial head and the radial notch of the ulna get in contact, and the annular ligament coated the anterior and posterior margins of the radial notch and the all circumference of the radial head (LaStayo & Lee, 2006; Morrey et al., 2018). The annular ligament bonds two bones to each other and stabilizes the radial head during the PS motion (Zimmerman, 2002). The PRUJ acts as ball bearing system due to the cylindrical shape of the proximal radius head (Kapandji, 2007; Soubeyrand et al., 2017). The peripheral edge of this structure rolls on the radial notch of the ulna, and this rolling motion allows the radius to rotate around the ulna (Kapandji, 2007). However, this rotation does not happen around a stable axis due to the structural differences between radius and the radial notch of the ulna. Thus, posterior and anterior translation of the radius head is observed in supination and pronation, respectively (Weiss & Hastings, 1992).

2.1.1.2 Distal Radioulnar Joint (DRUJ)

The DRUJ is the connection point of the distal ulnar head and the ulnar notch of distal radius head at the distal. The ulnar notch of the radius has a smooth surface that glides on the cylindrical-shaped ulna head (Doyle & Botte, 2003; Huang & Hanel, 2012; Kapandji, 2007; Soubeyrand et al., 2017). At the wrist, the DRUJ is separated from the radiocarpal joint via compiled ligament structure called triangular fibrocartilage complex cartilage (TFCC). Apart from separating the DRUJ and radiocarpal joint, the TFCC also bonds the ulnar notch of the radius and ulna head (Chidgey, 1995). It has an important role in stability of the DRUJ by restraining the possible spread between the radius and ulna heads at the distal end (Dumontier & Soubeyrand, 2013). The forearm rotation is mainly observed at the distal radioulnar

joint where the radius rotates around the mobile ulnar head (Rose-Innes, 1960). The anatomical structure of the DRUJ allows the radius and the ulna to rotate and glide on the surfaces of each other. The radius rotates around the mobile ulna while the ulna makes volar/dorsal and proximal/distal translation from supination to pronation (Chidgey, 1995; Dumontier & Soubeyrand, 2013; Palmer et al., 1982; Palmer & Werner, 1984; Tsai & Paksima, 2009).

2.1.1.3 Middle Radioulnar Joint (MRUJ)

At the MRUJ of the forearm, the radius and ulna shafts does not touch each other as we observed at the PRUJ and DRUJ. At this section, the radius and ulna shafts are boned via the IOM which is a multicomponent ligament covers the gap between the radius and ulna at the middle portion of the forearm (Adams, 2017; Dumontier & Soubeyrand, 2013; Soubeyrand et al., 2017). During the PS motion, the IOM, the annular ligament and TFCC stabilizes of the motion of the radius and ulna. It ensures the stability in both longitudinal and transverse directions of the forearm (Green & Zelouf, 2009). The IOM does not allow the expansion of the space between the radius and ulna shafts in the transverse direction, and the proximally translation of the radius together with the annular ligament and TFCC (Green & Zelouf, 2009; Rabinowitz et al., 1994). In addition to the stability of forearm, load transmission between the wrist and elbow is another important functionality of the IOM (Birkbeck et al., 1997; Markolf et al., 2000; McGinley & Kozin, 2001). Moreover, the radius and ulna have curved shape structures at the middle section of the forearm. The radius contains two curvatures called supinator and pronator curvatures which are the proximal one-thirds and distal two-thirds of the radius shaft, respectively. On the other hand, the ulna has anteriorly concave shape and S shaped curvature at sagittal and frontal planes, respectively (Soubeyrand et al., 2017). The curved shapes of the bones at the MRUJ have significant effect on the range of motion (ROM) of the PS motion (Matthews et al., 1982; Soubeyrand et al., 2017). The excessive curvature of the radius causes loss in the ROM of the forearm rotation (Matthews et al., 1982).

Besides, perfectly straight bone structure can cause a limitation in pronation motion (Soubeyrand et al., 2017).

2.2 Experimental Motion Analysis & Defining Pro/Supination Axis

The PS motion of the forearm is still an ambiguous topic that requires more investigation due to the complexity of the motion. The bone and joint physiology of the forearm causes a complicated longitudinal rotation of the forearm. Over the years, various studies tried to understand the mechanics behind the PS motion and fit the motion onto a proper rotation axis. The observations on the PS motion showed that the rotation axis and the longitudinal axis of the forearm are not coincident axes (Figure 2.3). In a common point, the previous studies found out that the PS rotation axis of passes from the radial head at the proximal end and the ulnar head at the distal end of the forearm (Fischer et al., 2001; Hagert, 1992; Hollister et al., 1994b; Matsuki et al., 2010; Nakamura et al., 1999; Oka et al., 2006; Ray et al., 1951; Tay et al., 2008, 2010; Van Sint Jan et al., 2002; Veeger et al., 1996; Youm et al., 1979). Although the previous studies agreed on which bone heads the rotation axis passes through at both sides, the exact location of the rotation axis was defined differently in these studies.

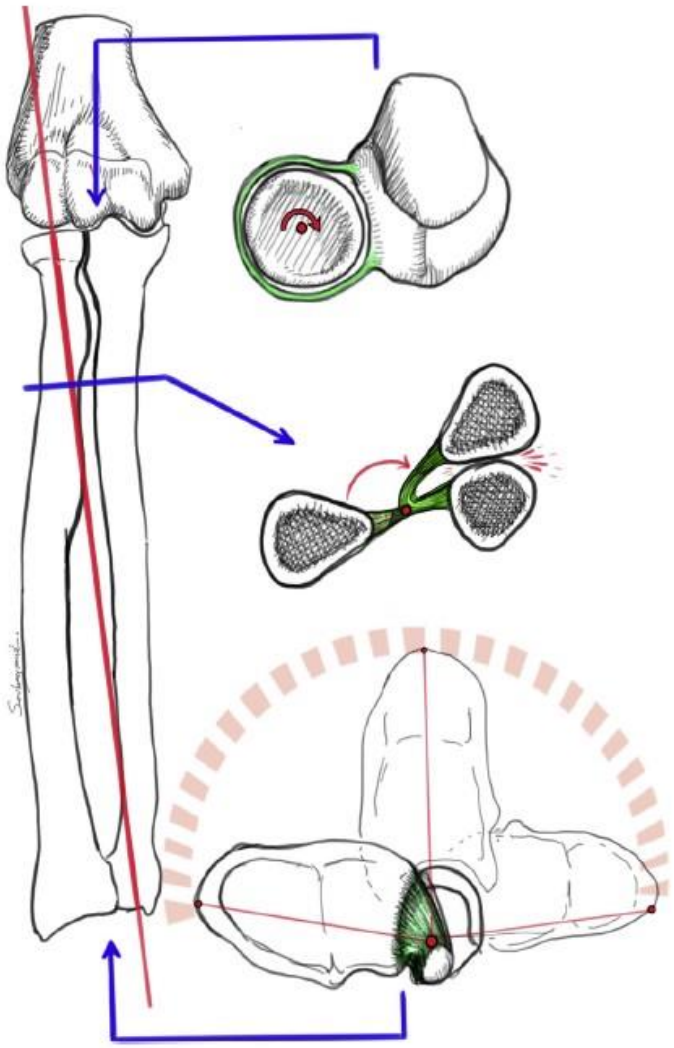

Figure 2.3 The rotation axis of the PS motion along the forearm (Soubeyrand et al., 2017)

The older studies, first, tried to understand the motion of the bones while the PS motion is happening. In a basic description, the PS motion was described as the rotation of radius around the fixed ulna. However, the elder studies showed this definition is an imperfect way of describing the PS motion. The investigations on the ulnar motion showed that ulna is not stationary during the PS motion, but it has flexion/extension and abduction/adduction movements together with the axial displacement (Anderson, 1901; Capener, 1956; Dwight, 1885; Heiberg, 1885; Ray et al., 1951). The studies showed that ulna moves laterally during pronation and

medially during supination, which is the opposite motion of radius (Capener, 1956; Ray et al., 1951). Besides, Ray et al. (1951) mentioned that the rotation axis of the forearm rotation might pass through somewhere between the fifth (little) finger and the index finger, and the rotation axis orientation may affect the range of ulnar motion. These studies showed that defining the proper rotation axis plays an important role to understand the motion of the ulna and the radius. To observe the motion of both radius and ulna, different motion capturing techniques were used by the previous studies, such as light-emitting diode (LED) (Youm et al., 1979), radiography (Chao & Morrey, 1978; Christensen et al., 1968), mechanical axis locators (Hollister et al., 1994b), 3D electromagnetic sensor (Veeger & Yu, 1996), magnetic resonance imaging (MRI) (Nakamura et al., 1999), computed tomography (CT) (Fischer et al., 2001; Oka et al., 2006; Tay et al., 2008, 2010; Van Sint Jan et al., 2002) and fluoroscopy (Matsuki et al., 2010) methods, and most of these studies were done at in vitro environment.

From the analysis done on the eight cadaver specimens, Youm et al. (1979) found out that the rotation axis of the PS motion passes from the centre of the capitulum at the proximal end and ulna head at the distal end. Youm et al. (1979) also claimed that the location of the tilted fixed rotation axis has a significant effect on the range of motion of the ulna bone. Their findings showed that if the rotation axis is located more radially, ulna performs a greater range of motion. The results that Hagert (1992) represented also supports the outcome of what Ray et al. (1951) and Youm et al. (1979) found about the ulnar movement during the PS motion. Hagert (1992) mentioned that ulna and radius change their orientations to allow the rotation of radius around ulna. Besides, his observations showed that the rotation axis of the forearm passes through the centres of the radial and the ulnar heads at the proximal and distal heads, respectively. Similar to these studies, Hollister et al. (1994) also fit the whole rotation on to a fixed axis. The rotation axis is defined as a single axis which lies between the centre of proximal radius head and the centre of the curvature of distal ulna head which is located nearby the ulnar styloid. Alongside the in vitro studies, Oka et al. (2006) did his experimentation on the six patients who has

posttraumatic radioulnar synostosis. Their analysis showed that the axis of rotation is passing approximately from the centre of radial head at the proximal side and the ulnar fovea at the distal side. Oka at al. (2006) also mentioned that although in vitro studies supply considerable understanding on the mechanics of forearm, these studies have limited evaluation on the mechanics of the motion since the muscle loads have to be simulated based on the estimations. Thus, the artificial fixation of bones might be required (Tay et al., 2008).

Although these studies tried to define a single axis for the rotation of the forearm, Veeger et al. (1996) stated that the rotation axis of the PS motion varies during the forearm rotation. This finding showed that the PS axis is not stationary, but its orientation changes together with the motion of the radius and ulna. Later on, the in vivo study of Nakamura et al. (1999) showed that the rotation axis is passing from the proximal radial head and distal ulnar head as demonstrated in previous studies (Hagert, 1992; Hollister et al., 1994b; Ray et al., 1951; Youm et al., 1979). However, Nakamura et al. (1999) showed that the location of the rotation axis is changing in a small range which was supported by the finding of Veeger et al.(1996). More recent in vivo studies also showed that the rotation axis orientation is different for each PS location (Tay et al., 2008, 2010). Tay et al. (2008) showed that from supination to pronation, the rotation axis moves from the ulnar to the radial region of the DRUJ, and the axis moves in the opposite direction at the PRUJ side (Figure 2.4). Besides, in their following study, Tay et al. (2010) represented the rotation axis orientation for five different subjects during the PS motion. They found that the path that the axis of rotation follows is different for each person, which affects the rotation capability of the forearm.

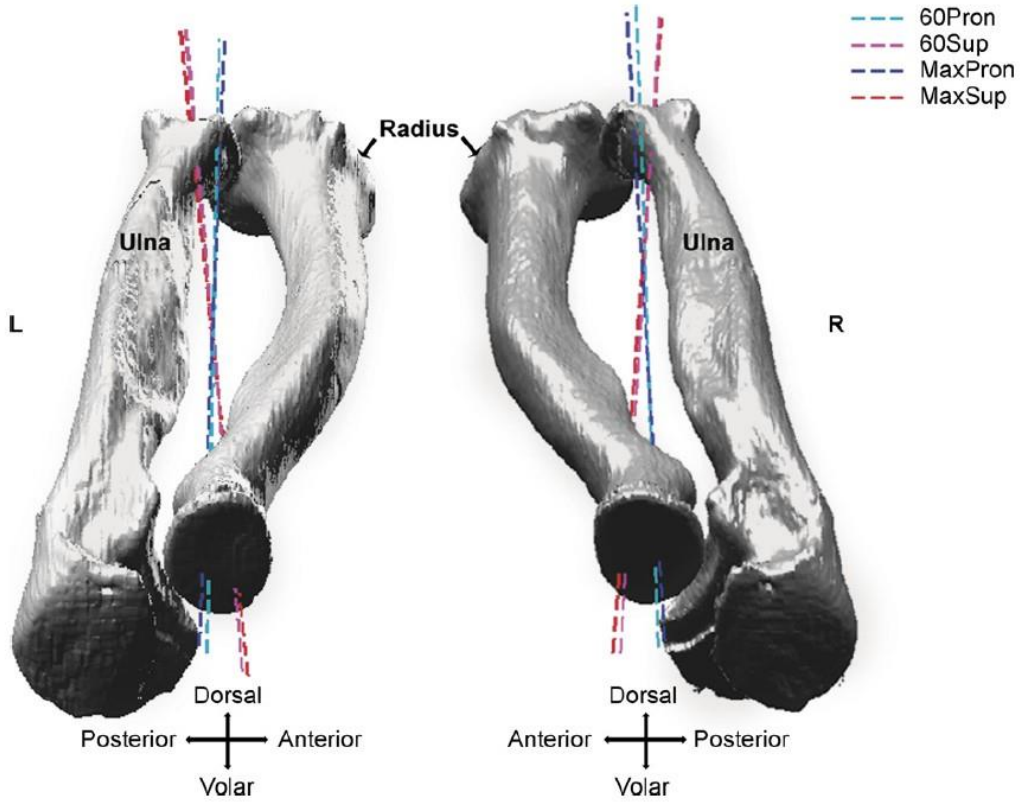

Figure 2.4 Rotation axis of the forearm for different PS poses (Tay et al., 2008)

2.3 Previous Kinematic Forearm Models

Accompanied with the motion analysis studies, researchers have been trying to build kinematic models of upper and lower limbs to investigate the kinematics and dynamics of the arm motion for many years. These kinematic models help us simulate bones' motion, the behaviour of joints, and the force distribution during any specific movement. In many modelling studies, which did not specifically focus on the PS motion, the forearm was modelled as a one-segment unit and the elbow joint as a universal joint so that it can do both the FE and PS motions (Fohanno et al., 2013, 2014; Kontaxis et al., 2009; Prokopenko et al., 2001; Raikova, 1992; van Andel et al., 2008; Zampagni et al., 2008). Even though these open-loop models provide an acceptable understanding of the forearm joint kinematics, they over simplify the complex functionality of the PS motion (Duprey et al., 2017). To

investigate the PS motion specifically, more detailed models are required (Laitenberger et al., 2015).

The first two-segment forearm model, which focuses on the PS motion, was proposed by Fick in 1904 (Duprey et al., 2017; Weinberg et al., 2000). The model consists of two L-shaped bodies with spherical joint connections at both sides of the bodies, and these spherical joint connections allow the rotation of the radius around the ulna representing PRUJ and DRUJ (Duprey et al., 2017). In this model, the ulnar motion was not included in the mechanism, and the rotation of radius occurred on a single axis that passes from the centres of spherical joints at both ends (Kecskeméthy & Weinberg, 2005; Weinberg et al., 2000). However, this model causes unrealistic hand abduction when the forearm rotates from supination to pronation (Duprey et al., 2017; Kecskeméthy & Weinberg, 2005). To eliminate the unrealistic hand abduction, the radioulnar variation was also included in the kinematic models which were presented in subsequent studies. Lemay and Crago (1996) build a dynamic forearm model to work on the functionality and the control of arm muscles during the forearm motion. They modelled the humeroulnar joint as a revolute joint, humeroradial joint as a ball and socket joint, DRUJ as a cylindrical joint, and the wrist as a universal joint. Although this model included the radioulnar variation inside the joint kinematics, the ulna segment was fixed, and the radius was rotated around the fixed ulna segment.

Weinberg et al. (2000) presented another kinematic forearm model, which has a mobile ulna segment contrary to Lemay and Crago's (1996) model. Weinberg et al. (2000) designed a spatial four bar mechanism where the links represent the radius, ulna, elbow and hand segments. In this model, elbow and hand segments are defined as distances between the bone centres at proximal and distal end of the forearm, respectively. The radius segment is connected to the elbow segment with a spherical joint, and the ulna can translate axially inside the prismatic joint at the end of the elbow segment. At the distal side, a universal joint connects the ulna segment with the radius and hand segment. The rotation axes of the universal joint are coincident with the ulna segment and the hand segment. The revolute joint, which have the axis

of rotation along the ulna, and the spherical joint at the proximal end of the radius segment allows the rotation of radius and hand segment around the ulna segment. Even though the axial translation of the ulna segment was included in the model, Kecskeméthy and Weinberg (2005) improved this model by adding the sway angle of the ulna and the virtual springs onto the joints allowing the ulnar motion.

Similar to these studies, Pennestrí et al. (2007) proposed another kinematic model to simulate forearm functionality of disabled people for optimization of automotive cockpits. They modelled the humeroradial joint as a spherical joint, the humeroulnar joint as a revolute joint, DRUJ as a guide joint and the wrist as a universal joint. Since the motion which was simulated in this study did not require the PS motion in a wide range, the sway angle of ulna was not included in the model. In addition to these models, Ramananarivo et al. (2017) developed a prosthetics forearm model where DRUJ was modelled as a 3-gear combination, and the radius and ulna were connected to the elbow segment of the prosthetics with spherical and revolute joints, respectively. Unlike the other models, the rotation axis of this model was defined between the elbow and wrist centres. Ramananarivo et al. (2017) mentioned that defining the rotation axis between the elbow and wrist centres is not proper biomechanically, however it is more practical in prosthetic design. In a most recent study, Yoon et al. (2019) proposed to model PRUJ and DRUJ with universal and revolute joint combinations within a four-bar mechanism. Their findings showed that this joint combination allows the rotation of both radius and ulna around a fixed rotation axis. Although both universal and revolute joints do not allow translation, the motion constraints of the universal joints at the proximal end causes the radioulnar variation during the PS motion.

In the extensive study published by Laitenberger et al. (2015), different forearm models are compared with each other. Laitanberger et al. (2015) mainly focused on modifying the forearm model that Kecskeméthy and Weinberg (2005) proposed. They embedded this model into an upper extremity model and changed the parameters according to the subjects who participated in motion data capturing. They also applied the same procedure for different forearm models which were previously

proposed in the literature (Fohanno et al., 2013; Kontaxis et al., 2009; Pennestrì et al., 2007; van Andel et al., 2008) to test the accuracy of their proposed upper limb model. The models were tested with the pure PS motion data, and the results showed that the closed-loop forearm mechanisms locate the hand more accurately than the open-loop forearm models. Besides, the greater range of motion of the hand was observed from the outcome of the closed-loop mechanism. According to the results obtained from the study, Laitenberger et al. (2015) mentioned that subject-specific closed-loop forearm models give more accurate results for the complex PS motion.

Table 1 summarizes all the previous models mentioned above. The table has information on how the PRUJ and DRUJ joints were represented in previous models and essential technical details of the models.

Table 2.1 Previous forearm kinematic models proposed in literature

References	PRUJ	DRUJ	Comments
Lemay and Crago (1996)	Spherical joint	Cylindrical joint	Radius rotates and translates around the fixed ulna
Weinberg et al. (2000)	Spherical & Prismatic Joint	Universal joint	Ulna is allowed to translate axially
Kecskeméthy and Weinberg (2005)	Spherical & Prismatic & Revolute Joint	3 Revolute joint combination	Ulna can both translate axially and sway laterally
Pennestrí et al. (2007)	Spherical joint	Guide joint	Lateral sway of the ulna is not included
Ramananarivo et al. (2017)	Spherical & Revolute joint	Gear train (consist of 3 gears)	The rotation axis is not accurate biomechanically
Yoon et al. (2019)	Universal & revolute Joint	Universal & revolute joint	Rotation around a fixed PS axis

CHAPTER 3

MODEL DEVELOPMENT

In the literature, different kinematic models were proposed to represent the PS motion of the forearm, which were discussed in the previous chapter. The results of these studies showed that the closed-loop models represent forearm rotation more accurately. In this sense, a novel two-segment closed-loop forearm model is proposed in this study to estimate the radius and hand orientation during the PS motion in a more realistic way.

3.1 Model Parameters and Joint Types

A generic forearm model is proposed, and the motion characteristics of the mechanism segments and the joints during the PS motion are discussed in this section. The proposed closed-loop forearm model consists of 3 links and 3 joints. These joints are spherical, prismatic and sphere in slot type of joints with 3, 1 and 4 degree-of-freedom (DOF), respectively. These joint combinations allow the mechanism to move in 3D space, and due to the spherical joint connections between the radius and the other links, the mechanism can be classified as a spatial mechanism. Although the joints have their own DOFs, the combination of the kinematic pairs creates constraints on the motion of mechanisms. Thus, the general degree-of-freedom equation (Equation 1) is used to define the DOFs of the mechanism.

$$F = \lambda(l - j - 1) + \sum_{i=1}^{j} f_i \tag{1}$$

where the DOF in space, number of links, number of joints and summation of the DOFs of joints are represented with $\lambda, l, j,$ and $\sum f_i$, respectively. The outcome of the formula shows that the proposed mechanism has 2 DOFs.

Figure 3.1 (a) and (b) shows the 2D front and side views, and (c) shows the 3D view of the mechanism. Unlike the previous models, the model includes the PS rotation axis as a part of radius link inside the model, and this axis is called as moving rotation axis (MRA). The DOFs of the mechanism are defined as PS angle, θ, and the orientation of the MRA at the distal end of the forearm, S_2. The PS angle is defined as the rotation around the MRA, and the orientational change of the MRA is allowed by the slot located at the distal end of the forearm. The link lengths of the proposed model are defined according to 50th percentile anthropometric data that Kecskeméthy and Weinberg (2005) were used to build their model. With this parametrization, the aim is to create a model that can mimic the motion capability of an average person. Table 3.1 provides the information on links and what they represent with the lengths of each link with respect to 50th percentile anthropometric data.

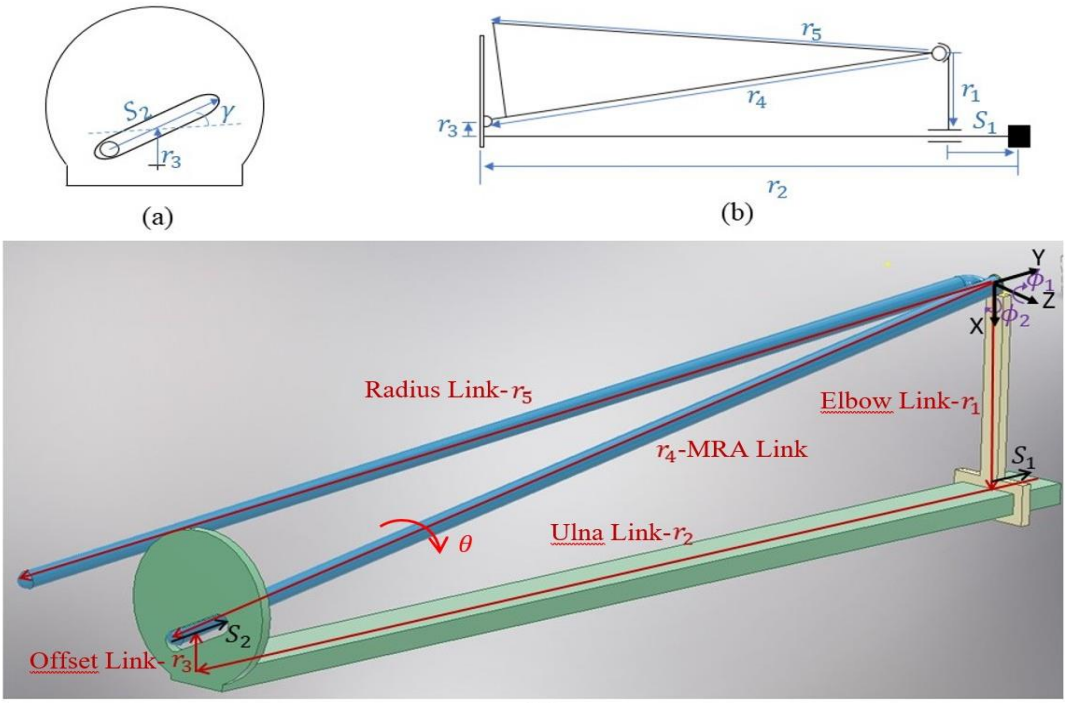

Figure 3.1 2D (a) front and (b) side views, and (c) 3D view of the proposed forearm model with vectorial representations of the links, joint variables and the global reference frame located on the HR joint

Table 3.1 Model parameters with vectorial representations, the locations, and magnitudes of each vector

Parameters	**Start Point**	**End Point**	**Value (mm)**
r_1 – Elbow Link	Proximal Radius Head (PRH)	Proximal Ulna Head (PUH)	25
r_2 – Ulna Link	Proximal Ulna Head (PUH)	Distal Ulna Head (DUH)	269
r_3 – Offset	Distal Ulna Head (DUH)	MRA Slot Centre	0.2
r_4 – MRA	Proximal Radius Head (PRH)	Distal MRA Head	270
r_5 – Radius Link	Proximal Radius Head (PRH)	Distal Radius Head (DRH)	269

Each link of the mechanism shown in Figure 3.1 represents the different anatomical segments of the forearm: the elbow, the ulna and the radius, and the motion of these links are analysed with respect to fixed global reference frame located at the humeroradial joint. Link 1, which is the elbow segment, connects the radius and the ulna segments to each other. This segment does not move during the PS motion, however it allows the motion of both the radius and the ulna segments. The length of this link is assumed as the distance between the proximal radius head (PRH) and proximal ulna head (PUH) centres (Kecskeméthy & Weinberg, 2005), and it is represented with the r_1 vector. At the upper end, the elbow segment has a socket that radius segment fits into it, and at the lower end it has a prismatic space that the ulna link can move inside, axially. The ulna segment, which is represented with r_2 vector, is a simple prismatic segment that represents the ulna bone of the forearm. At the proximal end of the mechanism, it is connected to the elbow unit with a prismatic joint, and it has a slot at the distal end of the forearm where the radius segment fits. Unlike the elbow and the ulna links, the radius segment has a triangular shape where one side represents the radius bone, r_5 vector, and the other represents the MRA, r_4 vector. The MRA side of the segment has a connection with the elbow and the ulna links at the proximal and distal ends, respectively. However, the centre of the MRA slot is not located at the centre of the distal ulna head (DUH). As discussed in the previous chapter, the rotation axis was determined in various locations at the distal end of the forearm. Hence, the slot is located with an offset from the DUH centre, which is represented with r_3 vector.

3.2 Modelling the Radioulnar Joint

At the proximal end of the model, the elbow link has spherical and prismatic joints with the radius and ulna segments, respectively. The anatomical studies showed that the PRUJ is like a ball bearing that allows the rolling motion of radius on the radial notch of the ulna (Kapandji, 2007; Soubeyrand et al., 2017), and the stability of the joint is obtained by the annular ligament which does not allow the lateral and medial

translation of the radius at the proximal end during the PS motion (Zimmerman, 2002). In this sense, a spherical joint is chosen for the connection of the radius segment with the elbow joint. This joint allows the rotational change of the segment in each direction which describes the gliding of the radius on the radial notch of the ulna. However, the translational motion of the MRA is not allowed at the PRUJ. Although Tay et al. (2008, 2010) mentioned that the location of the rotation axis is changing both at the proximal and distal ends, allowing the translational movement of the MRA at the proximal end requires to add another slot at the elbow which will complicate the model. The angular changes of the MRA around the z and x axes are represented with ϕ_1 and ϕ_2, respectively. These angular changes are observed due to the translational motion of the MRA at distal end. Since the spherical joint does not allow the translation motion, the rotation of the radius segment along z and x axes makes the translation of the MRA at the distal end possible. On the other hand, the rotation of the MRA along its longitudinal axis is defined as θ and this rotation represents the PS rotation of the forearm. It is one of the DOFs of the mechanism and during the analysis it is considered as one of the inputs. Apart from the radial motion, the investigations on the ulnar motion showed that the ulna has both translational and rotational motion during the PS movement to allow the greater range of motion for the radius bone (Anderson, 1901; Capener, 1956; Dwight, 1885; Heiberg, 1885; Ray et al., 1951). To prevent the model from geometrical constraints, adding the ulnar motion as part of PS motion is essential. At the proximal end, the axial translation of the ulnar segment is obtained by the prismatic joint between the elbow and the ulnar segment, and this axial transformation is represented with joint variable s_1 vector.

At the distal end of the model, the ulna link is connected to the radius segment with sphere in slot joint. This joint allows additional rotations along the x and z axes together with the rotation around the MRA. Tay et al. (2008, 2010) showed that the location of the rotation axis is changing at both ends with the change in bone orientations during the PS motion. They mentioned that the amount of linear change in the rotation axis shows the gliding amount between the radius and ulna, and the

linear change of the rotation axis might be used for the modelling of PRUJ and DRUJ. In the proposed model, the linear translational change of the axis at the distal end is only included with the slot located at the distal end the ulnar segment. Besides, Tay et al. (2008, 2010) showed that the rotation axis varies almost linearly in an oblique pattern. Their results showed that the rotation axis moving towards the ulnar side during the supination and the radial side during the pronation. Thus, the slot is located with an inclination angle, γ, and this inclination allows to orient the MRA from ulnar to radial side from maximum supination to pronation.

CHAPTER 4

KINEMATIC ANALYSIS

Kinematic analysis is performed to understand the motion behaviour of a particle, rigid body, or mechanism. To observe the motion behaviour of a particle or rigid body, global and local reference frames are defined in space. The global frame is the fixed frame that acts as a ground, and the local frame is attached to a particle or a point on a rigid body. The aim of the kinematic analysis is to observe the motion of the local frame with respect to global frame, and the outcome of this analysis determines the position, velocity, and acceleration of the local frame during the performed motion. In this study, the kinematic analysis is used to determine the position of the proposed mechanism. The displacement and angular changes at the joints are observed together with the orientation of the radius segment during the PS motion. Thus, this chapter explains the methodology to obtain the position and orientation change of the proposed model during the PS motion.

To perform the kinematic analysis, each local point is defined as a 4×1 homogenous vector in the form shown in Equation 2, and 4×4 homogenous transformation matrices (Equation 3) are used to define the rigid body motion (Özgören, 2019).

$$\bar{R} = \begin{bmatrix} \bar{r} \\ 1 \end{bmatrix} = \begin{bmatrix} r_x \\ r_y \\ r_z \\ 1 \end{bmatrix} \tag{2}$$

$$\hat{H} = \begin{bmatrix} \hat{C} & \bar{p} \\ 0 & 1 \end{bmatrix} = \begin{bmatrix} C_{11} & C_{12} & C_{13} & p_x \\ C_{21} & C_{22} & C_{23} & p_y \\ C_{31} & C_{32} & C_{33} & p_z \\ 0 & 0 & 0 & 1 \end{bmatrix} \tag{3}$$

Homogeneous transformation matrix represents the rotational and the translational motion of the local reference frame on a rigid body with respect to the global reference frame. $\hat{C}$, which is the orthogonal rotation matrix, describes the rotational change and $\bar{p}$ vector shows the translation change of the local frame according to the base reference frame. In Equations 4, 5 and 6, the representation of the rotational and the translational change around and along the x, y and z axes are shown, respectively.

$$\widehat{H}_{Rot,x} = \begin{bmatrix} \widehat{C_x} & 0 \\ 0 & 1 \end{bmatrix} = \begin{bmatrix} 1 & 0 & 0 & 0 \\ 0 & \cos\theta & -\sin\theta & 0 \\ 0 & \sin\theta & \cos\theta & 0 \\ 0 & 0 & 0 & 1 \end{bmatrix}, \tag{4a}$$

$$\widehat{H}_{Trans,x} = \begin{bmatrix} \hat{I} & \overline{p_x} \\ 0 & 1 \end{bmatrix} = \begin{bmatrix} 1 & 0 & 0 & p_x \\ 0 & 1 & 0 & 0 \\ 0 & 0 & 1 & 0 \\ 0 & 0 & 0 & 1 \end{bmatrix} \tag{4b}$$

$$\widehat{H}_{Rot,y} = \begin{bmatrix} \widehat{C_y} & 0 \\ 0 & 1 \end{bmatrix} = \begin{bmatrix} \cos\theta & 0 & \sin\theta & 0 \\ 0 & 1 & 0 & 0 \\ -\sin\theta & 0 & \cos\theta & 0 \\ 0 & 0 & 0 & 1 \end{bmatrix}, \tag{5a}$$

$$\widehat{H}_{Trans,y} = \begin{bmatrix} \hat{I} & \overline{p_y} \\ 0 & 1 \end{bmatrix} = \begin{bmatrix} 1 & 0 & 0 & 0 \\ 0 & 1 & 0 & p_y \\ 0 & 0 & 1 & 0 \\ 0 & 0 & 0 & 1 \end{bmatrix} \tag{5b}$$

$$\widehat{H}_{Rot,z} = \begin{bmatrix} \widehat{C_z} & 0 \\ 0 & 1 \end{bmatrix} = \begin{bmatrix} \cos\theta & -\sin\theta & 0 & 0 \\ \sin\theta & \cos\theta & 0 & 0 \\ 0 & 0 & 1 & 0 \\ 0 & 0 & 0 & 1 \end{bmatrix}, \tag{6a}$$

$$\widehat{H}_{Trans,z} = \begin{bmatrix} \hat{I} & \overline{p_z} \\ 0 & 1 \end{bmatrix} = \begin{bmatrix} 1 & 0 & 0 & 0 \\ 0 & 1 & 0 & 0 \\ 0 & 0 & 1 & p_z \\ 0 & 0 & 0 & 1 \end{bmatrix} \tag{6b}$$

To analyse the motion of the proposed model, two types of kinematic analysis are used in this study: Forward and Inverse kinematic analysis. In forward kinematic analysis, the position of the mechanism in space is defined according to the known

joint variables. On the other hand, the inverse kinematics is used to find the joint variables according to the known position of the mechanism in space. During kinematic analysis first the joint variables are found, and then the position of the radius side of the radius segment (distal radial head) is defined.

4.1 Inverse Kinematic Analysis

Before defining the position of the radius segment, the joint variables are needed to be verified. As mentioned in the previous chapter, the model has two DOFs which are the translation of the MRA in the slot defined at the distal end of the model, s_2, and the rotation around the MRA link, θ. For the inverse kinematic analysis, the position of the MRA vector is used to obtain the joint variables. Since s_2, is the input variable, the joint variables ϕ_1, ϕ_2 and s_1 can be determined according to the change of s_2. To obtain the analytical relation between s_2 and the joint variables, the loop closure equation of the model is built by using the successive rotations and translations of the local frames. In Figure 4.1, the schematic of the loop closure equations is shown. The abbreviations given in the Figure 4.1 show the origins of the local frames after each transformation/orientation, and what these abbreviations represents are shown in the Table 4.1. Moreover, the spherical joints allow the rotation of the local frame on each axis. Hence, to show that the origin of the local frame is not changing but the orientation is changing, superscripts are used to name the new local frame after the rotation as shown in Figure 4.1. The successive rotations and translations are shown with the rounded and flat arrows, respectively. On top of each arrow, on which axis the local frame is rotated or translated is shown together with the amount of the transformation. The mathematical representation of the loop closure equation is given in Equation 7 where T[a,b] and R[a,b] denotes a translation and rotation along axis a with an amount of b, respectively. Each rotation and translation between the local frames are defined with homogeneous transformation matrices, and loop closure equation of the mechanism is created by multiplying these homogenous transformation matrices as shown in Equation 7 and

8. To find the joint variables ϕ_1, ϕ_2 and s_1, the loop closure equation is solved according to the known input DOF of the mechanism, s_2, by using the inverse kinematic analysis. The analytical representation of ϕ_1, ϕ_2 and s_1 are given in Equations 9, 10 and 11, respectively. In the analytical representation of the ϕ_2 and s_1, sign ambiguities are appeared. These sign ambiguities might be plus or minus one according to the configuration of the mechanism. To fit the equations according to the correct configuration, the sign ambiguities are taken as plus and minus one in ϕ_2 and s_1 cases, respectively. Furthermore, as it can be seen in Figure 4.1, the MRA link has a rotational motion along z and x axes at both proximal and distal ends. The rotations at the distal end are expressed with ψ_1 and ψ_2, respectively. From the solution Equation 8, ψ_1 and ψ_2 are found mirror rotations of ϕ_1 and ϕ_2 at the distal side, respectively. The amounts are found equal however the directions are opposite to each other (Appendix C).

Table 4.1 Abbreviations & Subscripts to represent the origin of the local reference frame

Abbreviations	**Represents**
R	Radius
U	Ulna
HU	Humeroulnar joint
UMRA	Ulna- MRA joint (Slot that MRA that translates inside)
MRA	Moving Rotation Axis
P	Proximal End
D	Distal End

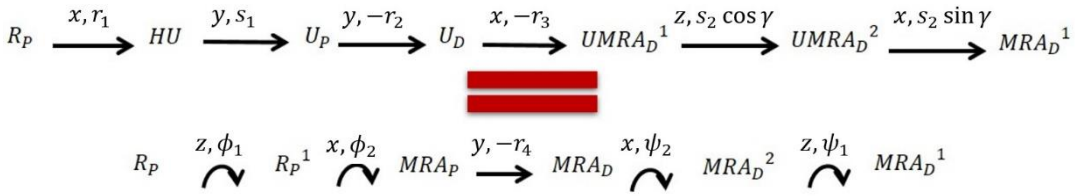

Figure 4.1 Schematic of the successive rotations & transformation in the loop closure equation of the proposed model

$$T[x, r_1] \times T[y, s_1] \times T[y, -r_2] \times T[x, -r_3] \times T[z, s_2 \cos\gamma] \times T[x, s_2 \sin\gamma] = R[z, \emptyset_1] \times R[x, \emptyset_2] \times T[y, -r_4] \times R[x, \psi_2] \times R[z, \psi_1] \quad (7)$$

$$\begin{bmatrix} 1 & 0 & 0 & r_1 \\ 0 & 1 & 0 & 0 \\ 0 & 0 & 1 & 0 \\ 0 & 0 & 0 & 1 \end{bmatrix} \cdot \begin{bmatrix} 1 & 0 & 0 & 0 \\ 0 & 1 & 0 & s_1 \\ 0 & 0 & 1 & 0 \\ 0 & 0 & 0 & 1 \end{bmatrix} \cdot \begin{bmatrix} 1 & 0 & 0 & 0 \\ 0 & 1 & 0 & -r_2 \\ 0 & 0 & 1 & 0 \\ 0 & 0 & 0 & 1 \end{bmatrix} \cdot \begin{bmatrix} 1 & 0 & 0 & -r_3 \\ 0 & 1 & 0 & 0 \\ 0 & 0 & 1 & 0 \\ 0 & 0 & 0 & 1 \end{bmatrix} \cdot \begin{bmatrix} 1 & 0 & 0 & 0 \\ 0 & 1 & 0 & 0 \\ 0 & 0 & 1 & s_2 \cos\gamma \\ 0 & 0 & 0 & 1 \end{bmatrix} \cdot \begin{bmatrix} 1 & 0 & 0 & s_2 \sin\gamma \\ 0 & 1 & 0 & 0 \\ 0 & 0 & 1 & 0 \\ 0 & 0 & 0 & 1 \end{bmatrix} =$$

$$\begin{bmatrix} \cos\emptyset_1 & -\sin\emptyset_1 & 0 & 0 \\ \sin\emptyset_1 & \cos\emptyset_1 & 0 & 0 \\ 0 & 0 & 1 & 0 \\ 0 & 0 & 0 & 1 \end{bmatrix} \cdot \begin{bmatrix} 1 & 0 & 0 & 0 \\ 0 & \cos\emptyset_2 & -\sin\emptyset_2 & 0 \\ 0 & \sin\emptyset_2 & \cos\emptyset_2 & 0 \\ 0 & 0 & 0 & 1 \end{bmatrix} \cdot \begin{bmatrix} 1 & 0 & 0 & 0 \\ 0 & 1 & 0 & -r_4 \\ 0 & 0 & 1 & 0 \\ 0 & 0 & 0 & 1 \end{bmatrix} \cdot \begin{bmatrix} 1 & 0 & 0 & 0 \\ 0 & \cos\psi_2 & -\sin\psi_2 & 0 \\ 0 & \sin\psi_2 & \cos\psi_2 & 0 \\ 0 & 0 & 0 & 1 \end{bmatrix} \cdot \begin{bmatrix} \cos\psi_1 & -\sin\psi_1 & 0 & 0 \\ \sin\psi_1 & \cos\psi_1 & 0 & 0 \\ 0 & 0 & 1 & 0 \\ 0 & 0 & 0 & 1 \end{bmatrix} \quad (8)$$

$$\emptyset_1 = atan_2\left(\frac{r_1 - r_3 - s_2 \sin\gamma}{r_4 \cos\emptyset_2}, \frac{r_2 - s_1}{r_4 \cos\emptyset_2}\right) \quad (9)$$

$$\emptyset_2 = atan_2\left(\frac{-s_2 \cos\gamma}{r_4}, \sigma_1 \frac{\sqrt{{r_4}^2 - {s_2}^2 \cos^2\gamma}}{r_4}\right), \sigma_1 = +1 \quad (10)$$

$$s_1 = r_2 + \sigma_2\sqrt{{r_4}^2 \cos^2 \emptyset_2 - (r_1 - r_3 - s_2 \sin\gamma)^2};\ \sigma_2 = -1 \quad (11)$$

4.2 Forward Kinematic Analysis

In the forward kinematics, the aim is to define the orientation of the radius segment and the distal radial head during the PS motion with respect to global reference frame located at the HR joint. Since anatomical studies showed that the hand unit is connected to the radius bone via radiocarpal joint (Doyle & Botte, 2003; Palmer et al., 1985), defining the orientation of the radius bone plays a significant role to obtain the correct hand orientation. It is known that the radiocarpal joint can perform flexion/extension motion and radial and ulnar deviation which may change the orientation of the hand in space (Palmer et al., 1985). However, in this study, such motions of the radiocarpal joint is not included and the hand is fixed to the radius, so that it rotates around the mobile ulna as part of radius during the PS motion (Duprey et al., 2017).

As mentioned in the previous chapter, the PS motion is one of the DOFs of the model, and it is defined as the rotation about the MRA. Therefore, to obtain the orientation of the radius vector, $\overrightarrow{r_5}$, the rotation of the radius segment about the MRA has to be considered for the forward kinematics. To perform this analysis, the orientation of the MRA vector, $\overrightarrow{r_4}$, has to be defined beforehand. Thus, the inverse kinematic analysis is performed for this purpose. After the inverse kinematic analysis, it is possible to obtain the joint variables ϕ_1 and ϕ_2 which define the orientation of the MRA vector together with the translation of the MRA, s_2, in the slot located at the distal end. By knowing the orientation of the MRA vector, it is possible to analyse the rotation of the radius vector, $\overrightarrow{r_5}$, around the MRA vector. To perform this rotation of the radius vector, the Rodriguez formula is used. The radius vector is defined as

the rotating vector and the MRA is defined as the rotation axis. In Equation 12, the rotation of the radius vector around the MRA is shown by using the Rodriguez formula (Özgören, 2019). Equation 12 gives the new orientation of the radius vector, $\overline{r_5}'$, after its rotation around the MRA vector, $\bar{r}_4$, with amount of performed PS angle, θ. The rotation matrix of this motion which represents the PS rotation is shown in Equation 13 where $\bar{r}_4$ is the column matrix of the rotation axis and θ is the amount of rotation which is PS angle. In both Equations, the tilde operator of a column matrix, $\tilde{r}$, represents the cross-product matrix (cpm) of the column matrix, $\bar{r}$. The tilde operator generates the screw symmetric matrix of the corresponding column vector, and the multiplication of the screw symmetric matrix with another column matrix represents the matrix form of the cross product between two vectors.

$$\overline{r_5}' = \bar{r}_5 \cos\theta + \tilde{r}_4 \bar{r}_5 \sin\theta + \bar{r}_4 \bar{r}_4^{\,t} \bar{r}_5 (1 - \cos\theta) \tag{12}$$

$$\hat{R}(\bar{r}_4, \theta) = \hat{I} \cos\theta + \tilde{r}_4 \sin\theta + \bar{r}_4 \bar{r}_4^{\,t} (1 - \cos\theta) \tag{13}$$

CHAPTER 5

MOTION ANALYSIS

Human motion analysis is an experimental process in biomechanics studies. It allows to identify both kinematics and kinetics of human body during a specific task that the subject of the experiment performs. As mentioned in the literature review, there are several methods to capture motion such as LED, radiography, 3D electromagnetic sensor, CT scans, MRI and fluoroscopy. These are useful methods to observe motion of a bones directly, however they are not capable to capture compound body movements due to the equipment limitations. To analyse the compound body motion, marker-based motion capturing technique is more applicable technique compared to the others since the subject can freely move to perform the given task. To collect motion data by using marker-based motion capturing technique, the markers should be placed onto the required body parts and the camera locations should be arranged as the way that each marker can be watched continuously during the experimentation. This experimentation provides the position change data of each marker within a frame interval. Thus, the location of each body segment in space with the change in their velocity and acceleration during the given task can be found. By knowing all the position, velocity, and acceleration changes of the body parts, it is possible to calculate the joint angles and joint forces during the motion.

This chapter explains the motion data that is used in this study, and how the segments and frames are defined in MATLAB environment. The motion analysis is used to validate the motion characteristics of the proposed model and the comparison is presented in the following chapter.

5.1 Motion Data

The motion data that is used in this study is obtained from the open-source whole-body human motion database of the Karlsruher Institut für Technologie (Mandery et al., 2015). The identification number of the motion data is 1331, and the subjects are Subject 3 and Subject 912. The scenario of the task is explained as one of the subjects is a mechanic and the other is a robot. Initially the mechanic climbs on the ladder for two steps and the robot gives the cooking spoon to him. Then the mechanic uses cooking spoon as a screwdriver and performs the screw manipulation for 3 times. Since the PS motion is considered in this study, only the frame interval where the mechanic performs the screw manipulation is taken into account. From the cameras used in the experimentation, the motion is collected and stored in C3D file format. The motion is simulated in the motion analyser software Mokka. The Mokka software presents the visual of the motion by placing the markers on the space as shown in Figure 5.1.

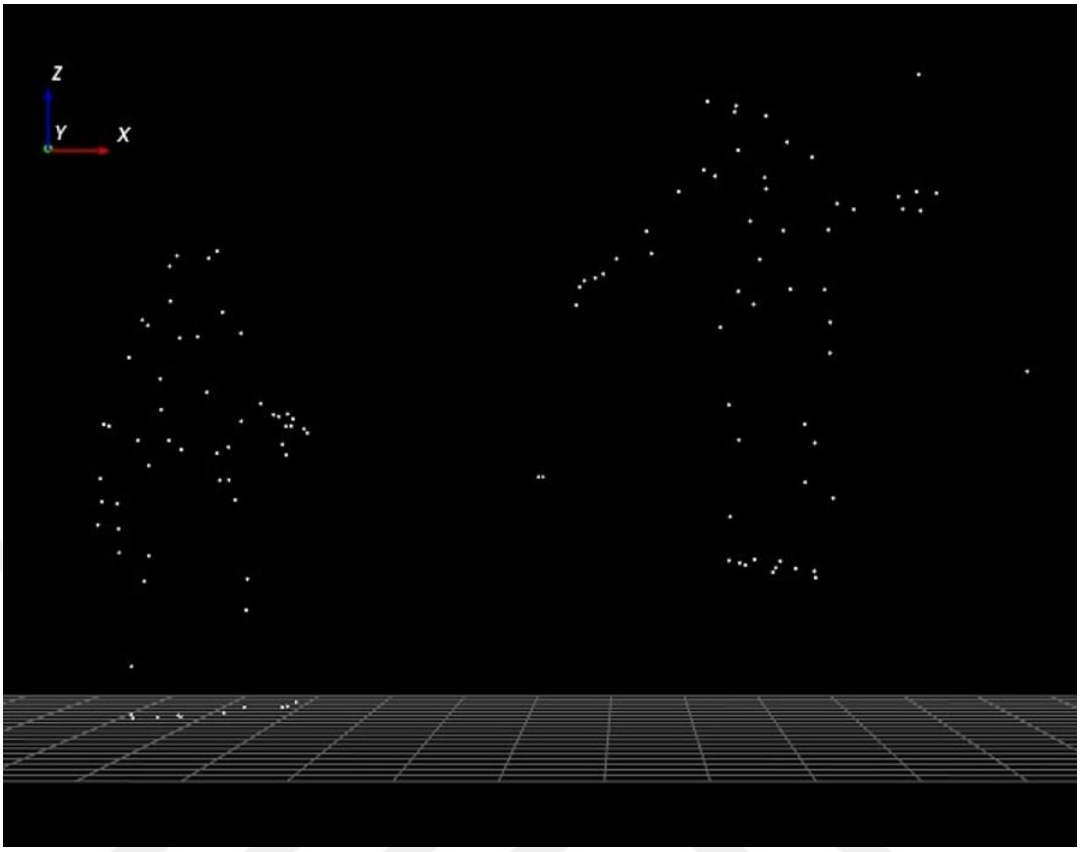

Figure 5.1 Motion simulation in Mokka Software

Figure 5.2 shows the markers of upper body which are placed on the motion capturing suit that each subject wears during the experiment. These marker sets are used to define local reference frame for each segment. Since the mechanic subject performs the screw manipulation with his right hand, the right portion of the upper extremity is analysed during the motion. Thorax, shoulder, humerus and forearm segments are defined according to the STRN, CLAV, C7, T10, RSHO, RAEL, RWTS and RWPS markers.

Figure 5.2 Upper body marker set placed on a subject. (a) shows the markers located on the front side and (b) shows the back side (Mandery et al., 2015)

5.2 Locating Joint Centres & Defining Local Frames

Locating the joint centres and defining the local frames of each body segments is essential to identify the relative motions between the body segments. In this study, the joint centres and local frames are located according to the VICON Body Language algorithm. The PS angle change during the screw manipulation and the motion pattern of radius with respect to the humerus frame is obtained in MATLAB environment.

To build the body segments, the data obtained from STRN, CLAV, C7, T10, RSHO, RAEL, RWTS and RWPS markers are defined in MATLAB, and the Thorax centre, Right Shoulder Joint Centre (RSJC), Right Wrist Joint Centre (RWJC) and Right Elbow Joint Centre (REJC) are located according to marker orientations.

Thorax is defined according to STRN, CLAV, C7 and T10 markers. From these 4 markers 2 different vectors and the local frame centre of thorax are defined. One of

these vectors is defined between upper and lower midpoint, and the other is defined between front and back midpoint of the thorax. The midpoints of upper, lower, front, and back sides of thorax are located at the midpoints of CLAV and C7, STRN and T10, CLAV and STRN, and C7 and T10, respectively. The vector from upper to lower midpoints is matched as the z axis of the thorax local frame, and the vector between front and back side is used to define y axis. The cross product between upper-lower and front-back vectors gives the unit vector of y axis which is towards the left arm, and the cross product between y and z axes defines the x axis which is towards the back side of the thorax. After the unit vectors are defined, the local frame centre of the thorax is placed to the midpoint of CLAV and C7.

Shoulder joint centre is defined according to the thorax local frame. Since the RSHO marker does not give the exact location of the joint centre of the right shoulder, two different parameters ISHO constant and lateral shoulder offset are also defined in the algorithm to locate the RSJC. ISHO is a constant value which shows the vertical offset of joint centre and lateral shoulder offset is an anthropometric measurement taken from the subject which shows the lateral difference between the marker and the joint centre. To define the exact location of the shoulder joint centre, these two distance vectors are summed and transferred to the thorax frame and their summation with RSHO marker locates the RSJC. After the shoulder joint centre is located, the unit vectors of the shoulder frame can be defined according to the RSJC, Thorax local frame centre and unit vectors. The unit vector of the z axis is located on the direction of the vector from the RSJC to Thorax frame centre. To define the x axis of the local shoulder frame, the cross product of the z axis of shoulder frame and the inverse z axis of the thorax frame is calculated, and then the cross product of the z and x axes of the shoulder frame is taken to define the y axis of the frame.

To define the elbow joint centre, the wrist joint centre has to be defined together with an initial humerus frame. The RWJC is simply defined as the midpoint of RWTS and RWPS markers which are located at the radial and ulnar styloid, respectively. The origin of the initial humerus frame is placed on the RAEL marker. To define the z axis of the initial humerus frame, a vector between RSHO and RAEL marker is

defined and shifted along the y axis of the thorax as the half amount of the summation of elbow thickness and marker diameter. The z axis of the initial humerus frame is fitted on this shifted axis. Similar to the thorax frame, another vector between RAEL marker and the RWJC is defined and its cross product with the z axis gives the y axis of the humerus frame. After y and z axes are founded, the x axis is oriented according to their cross product.

After obtaining the RWJC and the initial humerus frame, the REJC is located by using a special function for the VICON software which is called as the CHORD function (Vicon Motion Systems, 2010). The CHORD function uses 4 different inputs to define the required joint centre. As shown in Figure 5.3 (a), the previously determined joint centre, the joint marker which has a perpendicular offset to the vector between the previous joint centre and the required joint centre, a plane defining marker, and the magnitude of the offset between the real marker has to be entered as the inputs of the CHORD function. The function uses these inputs to define the position of the required joint centre in the space. As shown in Figure 5.3 (b), the CHORD function creates a plane by using the previous joint centre, joint marker and plane defining marker. Then, the function draws a half circle on that plane which passes from previous joint centre and joint marker where the diameter of the circle is set to be the vector between these two points. Inside that half circle, the function draws a right-angled triangle where the short edge has the length of the offset defined in the function, and the corner which has the 90º angle is the required joint centre that has to be on the circle. Since the length of shortest and the longest sides are known, the angles of triangle can be determined by geometry. At the final step, the function defines the unit vector of the x axis in the direction of the vector defined from the joint marker and the known joint centre. It takes the cross product of the normal unit vector of the plane and the unit vector of the x axis to define the unit vector of the y axis of the plane. The origin of the frame is located on the joint marker, and location of the required joint centre is found according to the local frame on the joint marker. Thus, the location of the required joint centre is defined on the plane where half circle lies. After the joint centre is defined on the plane, the

homogeneous transformation matrix between the local frame and the global reference frame is used to find the of the joint centre according to the global reference frame.

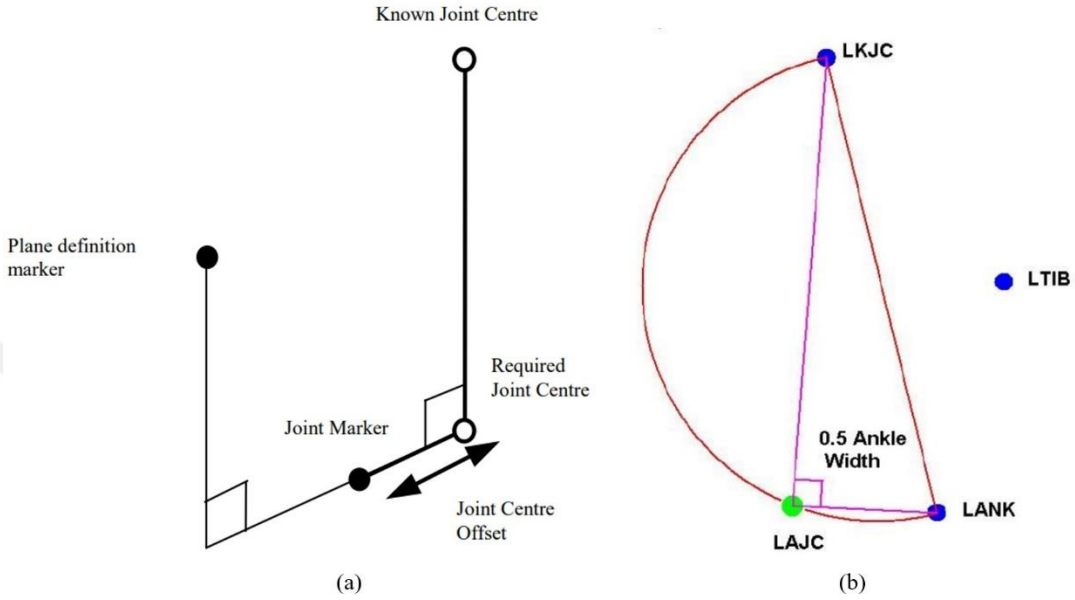

Figure 5.3 (a) shows the inputs of the CHORD function and (b) shows the geometrical representation of the CHORD function (Vicon Motion Systems, 2010)

At the final step, the local coordinate frames of the humerus and the forearm segments has to be defined. Compared to the initial local frame of the humerus, the origin of the humerus local frame is located at the REJC, and the z axis of the humerus frame is matched with the vector from RSJC to REJC. To find the x and y axes of the humerus frame, first the cross product of the z axis and vector defined from REJC to RAEL, and then the cross product of z and x axes is taken, respectively. Similar to the humerus frame, the forearm frame is located on the RWJC, and the z axes is defined from the REJC to RWJC. The cross product of the z axis and the vector from RWPS to RWTS gives the x axis of the forearm frame, and the y axis is defined according to the cross product of z and x axes. Although forearm consists of two different rigid bodies, for simplicity, radius and ulna considered as a single rigid body and the forearm axis is defined between the REJC and RWJC.

In Figure 5.4, the MATLAB plot of the body segments and the local frames located at the joint centres are shown for the initial frame of the taken data. The solid blue line is drawn from the origin of global frame to the centre of thorax frame to show the orientation of the body of Subject 912. Apart from that, the dashed blue lines connect the markers, and dashed-dot lines in different colours connect the markers the joint centres. Dash-dot lines are drawn in black, red, and magenta colours and they represent the clavicle, humerus and forearm segments, respectively. Hence, the unit vectors of each local frame are shown with green, blue, and red arrows which represent the unit vectors of the x, y, and z axes of each local frame, respectively. Table 5.1 shows the required anthropometric measurements of the Subject 912 and the marker diameters.

Table 5.1 Anthropometric measurements of the subject 912 and the marker diameters

Parameter	**Value (mm)**
Lateral Shoulder Offset	60
Elbow Thickness	110
Marker Diameter	14

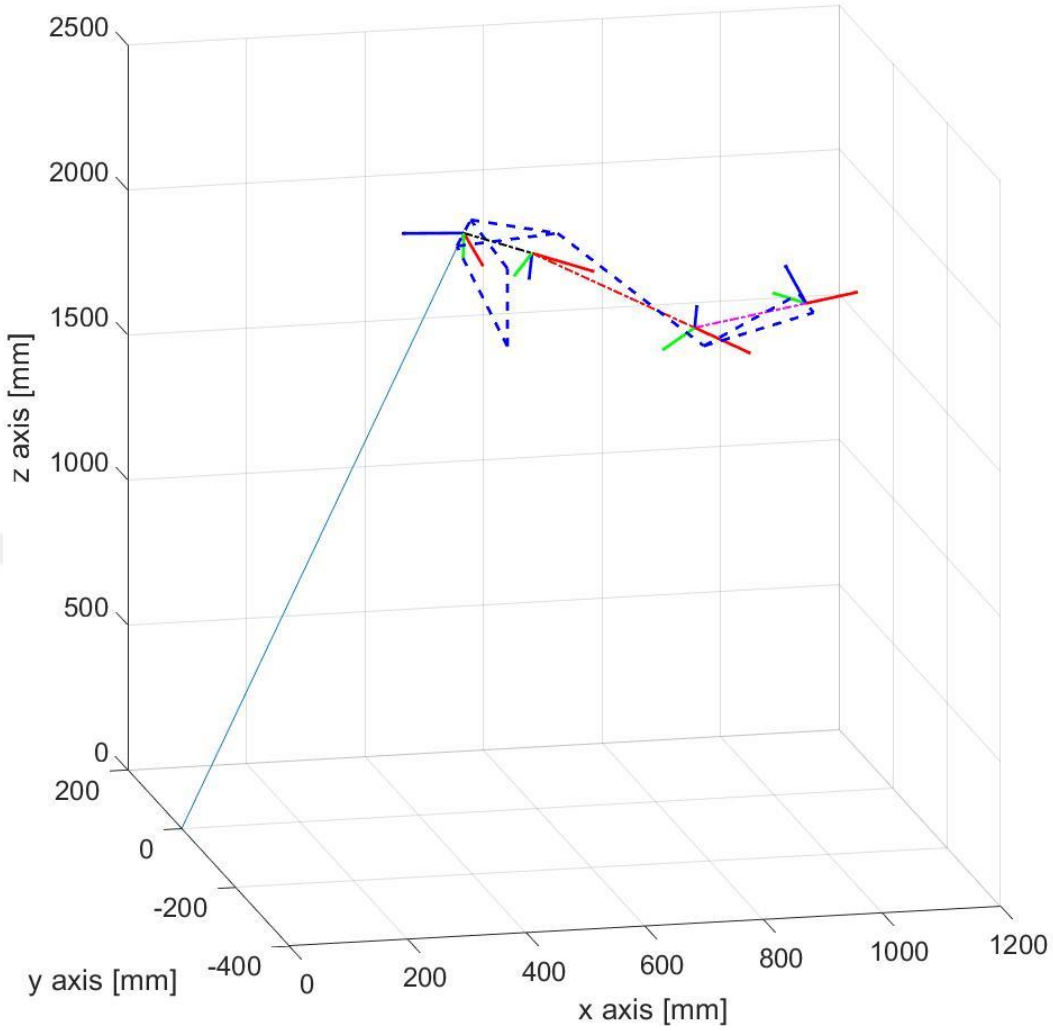

Figure 5.4 The MATLAB plot of the body segments and the local frames located at the joint centres at the initial frame of the motion data

5.3 Kinematic Analysis of the Motion Data

As mentioned before, since the PS movement of the forearm is the main focus of this study, the frame interval where Subject 912 performs screw manipulation is taken under consideration during the analysis. During the kinematic analysis, the PS range and the pattern that RWTS marker follows are observed within the specified frame interval.

To observe the angular changes between humerus and the forearm arm, the rotational changes between local coordinate frames of each body segment has to be analysed by using the inverse kinematic analysis. The relation between ground, elbow and wrist is defined by the homogeneous transformation matrices, and solution for homogeneous transformation matrix between elbow and wrist is shown in equation 14. To define the rotational changes between the frames, the Rotation matrix between each joint centre and ground is found by using the Equation 15. The dot product of each unit vector shows the cosine of the angular change between each axis. The translation side of the transformation matrix is simply defined with the location of the joint centre with respect to global frame.

$$\widehat{H}_{ew} = \left(\widehat{H}_{ge}\right)^{-1} \widehat{H}_{gw} \tag{14}$$

$$\begin{aligned} \hat{C} &= \begin{bmatrix} u_i^a & u_j^a & u_k^a \\ v_i^a & v_j^a & v_k^a \\ w_i^a & w_j^a & w_k^a \end{bmatrix} \begin{bmatrix} u_i^b & v_i^b & w_i^b \\ u_j^b & v_j^b & w_j^b \\ u_k^b & v_k^b & w_k^b \end{bmatrix} \\ &= \begin{bmatrix} \cos\theta_{11}{}^{(a,b)} & \cos\theta_{12}{}^{(a,b)} & \cos\theta_{13}{}^{(a,b)} \\ \cos\theta_{21}{}^{(a,b)} & \cos\theta_{22}{}^{(a,b)} & \cos\theta_{23}{}^{(a,b)} \\ \cos\theta_{31}{}^{(a,b)} & \cos\theta_{32}{}^{(a,b)} & \cos\theta_{33}{}^{(a,b)} \end{bmatrix} \end{aligned} \tag{15}$$

Since it is known that the PS motion is the longitudinal rotation of the forearm, the rotation along the z axis of the forearm frame is observed during the specified frame interval. After the transformation matrix between the REJC and the RWJC is obtained, the PS angle is defined by the Equation 16. Together with the PS angle range, the relative motion of the vector between REJC and RWTS with respect to humerus frame is also observed to validate the motion capability of the proposed forearm model.

$$\theta_{PS} = atan_2\left(\frac{c_{12}}{-\sqrt{c_{11}{}^2 + c_{12}{}^2}}, \frac{c_{11}}{\sqrt{c_{11}{}^2 + c_{12}{}^2}}\right) \tag{16}$$

CHAPTER 6

RESULTS & DISCUSSION

In previous chapters, the mechanism structure of the proposed model, methodology of inverse and forward kinematic analysis applied on the model and how PS motion is observed from the motion data are explained in detail. In this chapter, the results of the model and motion analysis is presented and discussed according to the previous studies.

As mentioned in Chapter 3, the inputs of this model are the translation of the MRA inside the slot defined at the DRUJ, s_2, and the rotation of the radius segment around the MRA, θ. The translation of the MRA inside the slot represents the change in the orientation of rotation axis of the forearm at the distal end, and the rotation around the MRA is defined as the PS rotation. Table 6.1 shows the variation amount of the inputs with the defined boundaries. The change in both inputs assumed linearly and the step sizes are changed synchronously. The slot length is defined as 10mm, and the s_2 varies from -5mm to 0 in supination, and 0 to 5mm in pronation. In the meantime, the PS angle, θ, has the 180º range where -90º to 0 side is defined as the supination and 0 to 90º side as the pronation motion. In addition to the input variables, the model tested for four different slot inclinations. Since Tay et al. (2008) showed that the PS axis moves in an almost linear, inclined pattern which varies from the ulnar to radial region from supination to pronation, the inclination angle, γ, is introduced to the model. Furthermore, Tay et al. (2010) also found that the pattern location, inclination and length changes from person to person, however almost linear patterns were observed for each subject of the their study. Thus, the proposed model tested under four different inclination angles, γ, to observe how outcomes of the model changes for the subject specific conditions. The results are obtained when γ is located at 0, 30º, 60º and 90º.

Table 6.1 Variation amount of the inputs with their boundaries

Input Variables	Values	Step Size
$s_2\ (mm)$	From -5 to 5	0.06
θ (°)	From -90 to 90	1

Figures 6.1, 6.2 and 6.3 shows the changes of joint variables ϕ_1, ϕ_2 and s_1 during the PS motion for the four different γ angles, respectively. (a), (b), (c) and (d) parts of each Figure represent the results of the specified joint variable when γ is equal to 0, 30º, 60º and 90º, respectively. The results presented in Figure 6.1 shows that the range of ϕ_1 changes from 0.0009º to 2.1312º with the increase in inclination angle. When the γ is set to 30º, 60º and 90º, the increase of ϕ_1 is observed in linear behaviour, and the range of ϕ_1 increases directly proportional to the increase in γ angle. However, for the slot located without an inclination, ϕ_1 is obtained in parabolic pattern changes within a quite small range compared to the inclined slots. In contrast to change in the range of ϕ_1, increase in the range of ϕ_2 is found inversely proportional to the increase of the slot inclination as it can be seen in Figure 6.2. The maximum range of ϕ_2, 2.12º, is observed when the slot is oriented without an inclination, and its range decreases with the increase of γ. When the γ angle is set to 90º, no change is observed in ϕ_2. Although the increase of ϕ_1 and ϕ_2 is observed inversely proportional, the ranges of both angles observed considerably small and close to each other due to the geometry of the mechanism. Since the link lengths of the radius, ulna and MRA are notably greater than the length of the elbow link and the MRA slot, obtaining small ranges for ϕ_1 and ϕ_2 is an expected outcome of this analysis. Besides, the relation between the change in the ranges of ϕ_1, ϕ_2 and the slot inclination is also found meaningful. To obtain the maximum angular change along the z or x axes, the slot has to be oriented perpendicular to them. When the slot is located without an angle, it is become perpendicular to x axis where the maximum range for the ϕ_2 is obtained. Likewise, when the slot is located with 90º, the

maximum range for ϕ_1 is found. These results shows that the findings of the inverse kinematic analysis are in accordance with the geometrical constraints of the model.

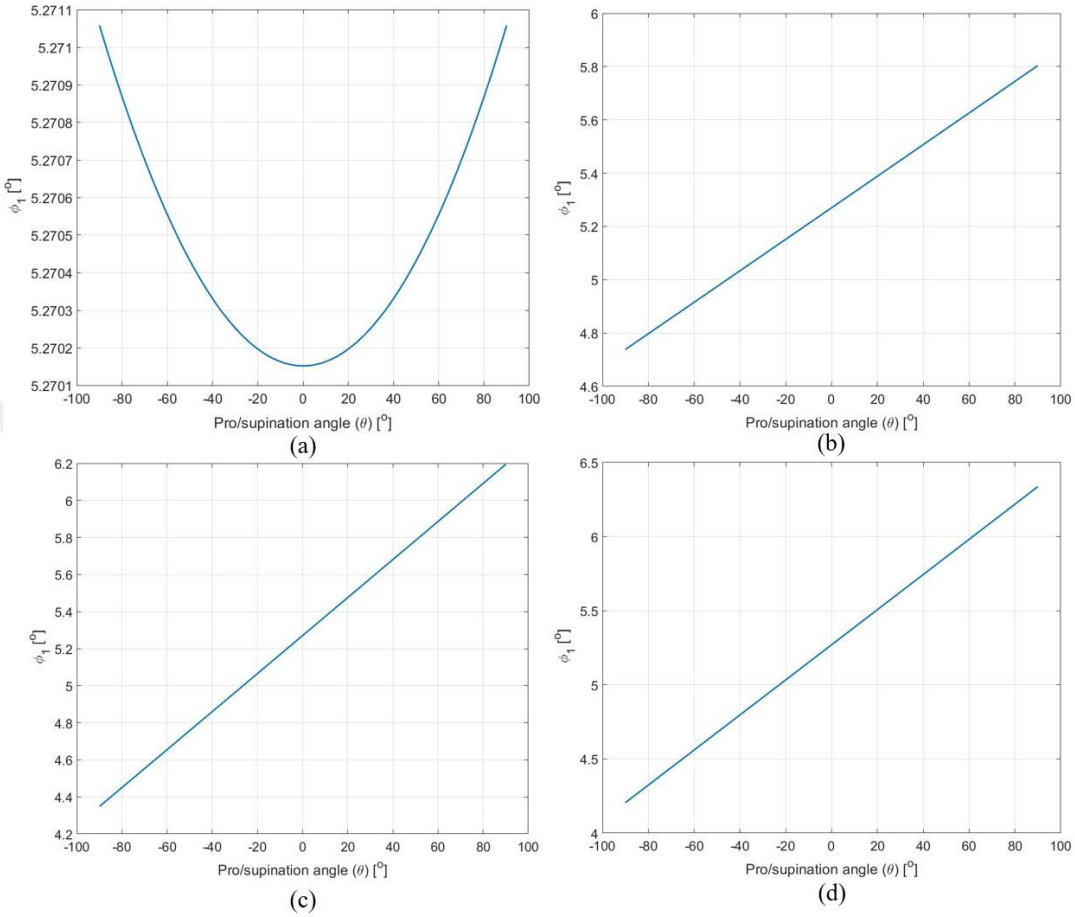

Figure 6.1 The rotational change around the z axis at the spherical joint of the PRUJ when (a) γ=0, (b) γ=30º, (c) γ=60º, and (d) γ=90º

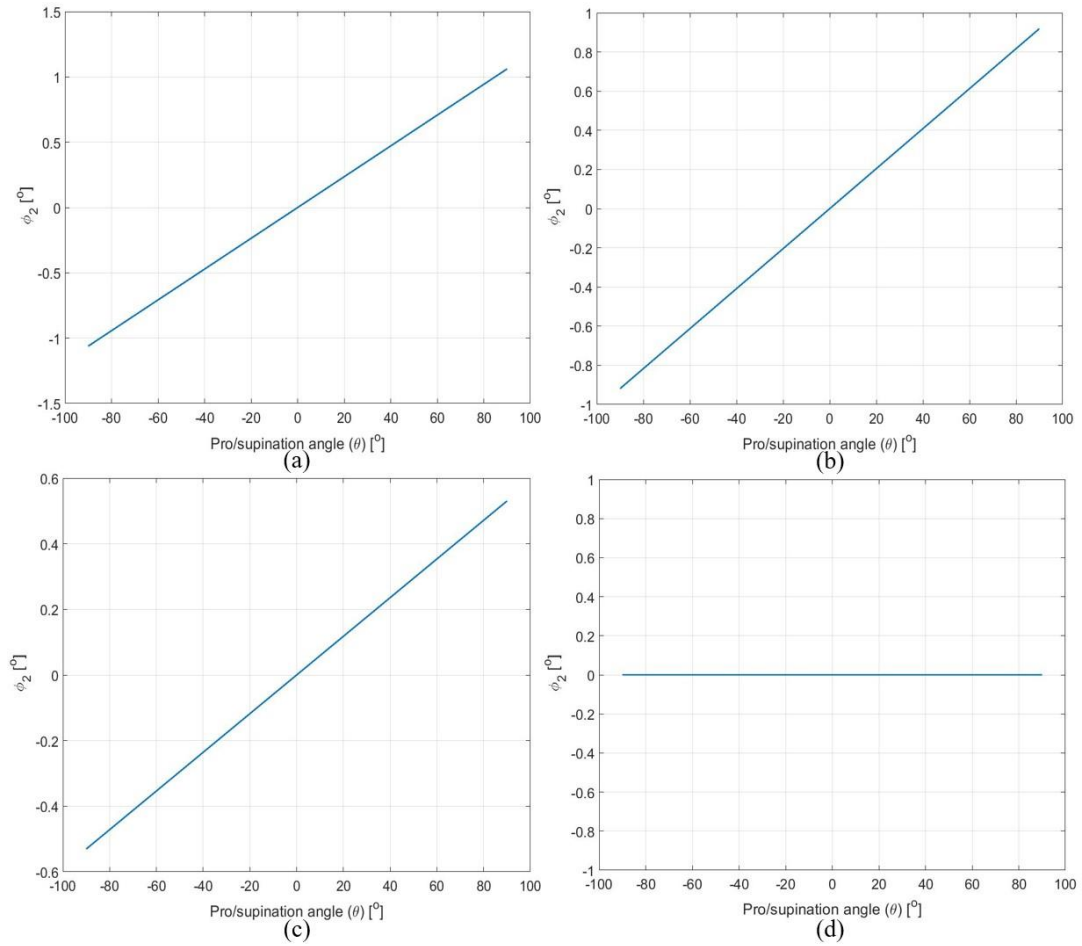

Figure 6.2 The rotational change around the x axis at the spherical joint of the PRUJ during the PS motion when (a) γ=0, (b) γ=30º, (c) γ=60º, and (d) γ=90º

Figure 6.3 shows the ulnar translation of the ulna link, s_1, during PS motion. Results show that the axial translation range is increasing with the increase of the slot inclination angle. The lowest range of 0.047mm and the maximum range of 0.922mm are obtained when the slot is located at the extreme points 0 and 90º, respectively. Similar to the ϕ_1, the change of s_1 is observed in a parabolic pattern when the γ is set to 0. However, ulna varies proximally from maximum supination to pronation, anatomically. For the other inclination angles, the ulna follows an almost linear trend in proximal direction. With the increase in inclination, the axial translation of the ulna is also increased. From 30º to 90º γ angle, ulnar translation

changed from 0.46mm to 0.922mm. Despite the difference in the range, the trend for each observed quite similar.

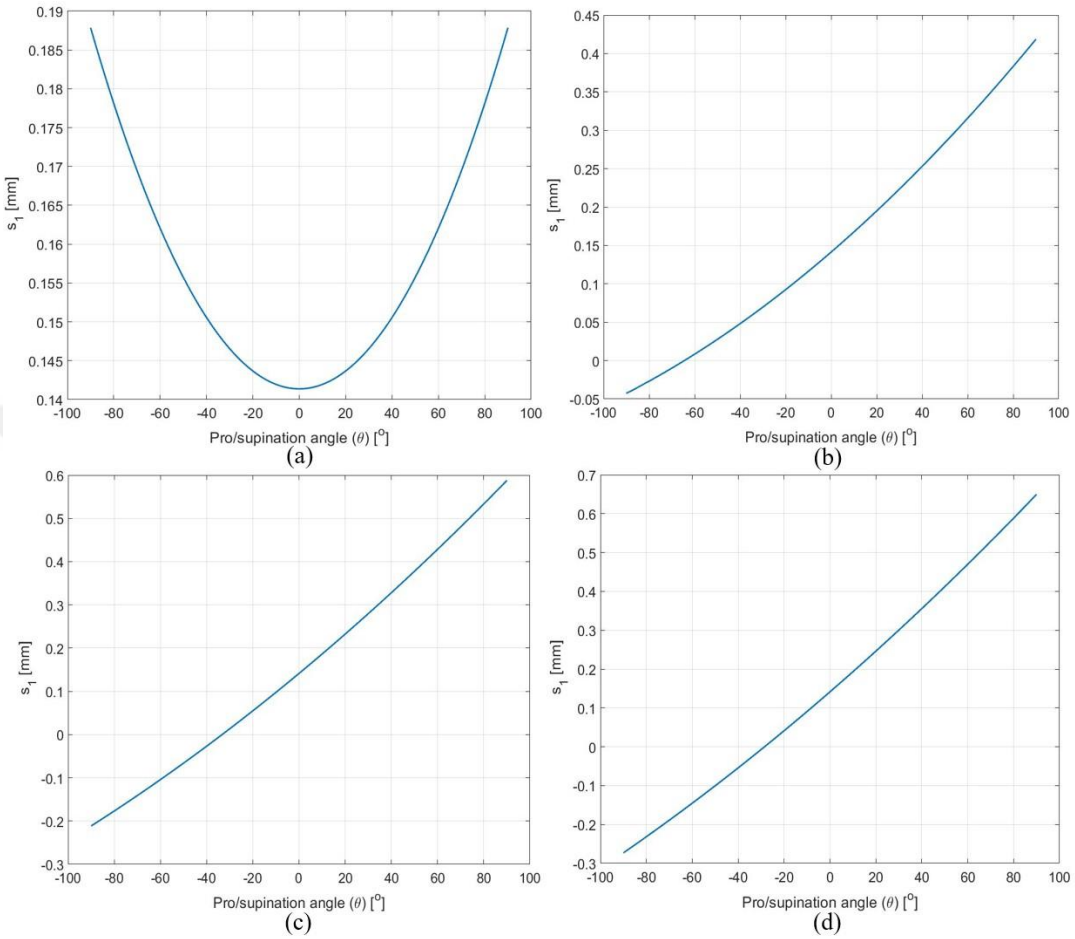

Figure 6.3 The axial translation of the ulna link during the PS motion when (a) γ=0, (b) γ=30º, (c) γ=60º, and (d) γ=90º

As expressed in the Chapter 4, forward kinematic analysis is applied to find the orientation of the radius vector, r_5. The PS motion input is defined as the rotation along the axis of the MRA vector, and the trajectory of the radius vector on the frontal plane (z-x plane) while it is rotating around the MRA vector is presented in Figure 6.4 for each inclination angle. Besides, the location of the radius head on the frontal plane and the range of motion at maximum supination and pronation poses for each inclination angle is presented in Table 6.2.

Although the PS rotation around the MRA is defined as 180º which varies from -90º to 90º, the range of motion of radius vector is observed less than the defined PS angle. The results show that the change in the inclination angle has a significant effect on the range of motion (ROM) of the radius head as well as its trajectory in space. The ROM of the radius vector and the inclination angle of the slot has a directly proportional relation. The minimum ROM of the radius vector is obtained as 166º (83º Supination+83º Pronation) where the γ is equal to 0, and it shows an increasing trend up to 176.6º (95.4º Supination+81.2º Pronation) where the γ is 90º. Even though the total ROM increases from 0 to 90º inclination, the ranges of supination and pronation poses change differently. When the slot is located without an inclination angle, the supination and the pronation poses are observed symmetric, and their ranges are founded as 83º. However, the ranges and the trajectories become unsymmetrical with the increase in γ. The supination range shows an increasing trend similar to the total range which varies from 83º to 95.4º from 0 to 90º inclination. Nevertheless, nonlinear parabolic change is observed in pronation pose. The maximum ROM of pronation pose is observed when there is no inclination, and it decreases first then increases somewhere between 30º to 90º with the increase in inclination angle. Among the four tested γ angle, the minimum ROM for pronation pose is obtained as 79.2º. Since the same behaviour is observed for the total and supination ROM, a regular behaviour was expected to obtain for the change of pronation range as well. However, the second largest range (81.2º) for the pronation is observed when γ is set to 90º. These results show that pronation and supination phases of motion has quite different characteristics. Although the supination ROM is found quite dependent on the change in the axis pattern, the pronation phase is not affected from the change in axis pattern as much as the supination phase. The ROM of pronation phase is deviated in a small range where the supination ROM increases rapidly with the increase of the inclination angle. Thus, to be able to understand the mechanics of each phase, it might be better to investigate them separately. By this way, the limitation factors of the PS motion might be understood more clearly.

In addition to the ROM of forearm, the trajectory of the radius head is also important to understand the motion characteristics. The model outcomes show that the change in slot inclination effects the pronation and supination sides differently. In pronation pose, the main difference among patterns is occurred along the z axis. From 0º to 90º of γ angle, results shows that the radius head is located more towards the centre where its shifted 9.8mm. On the other hand, along the x axis the radius head location changed within 1.9mm anterior-posterior interval. At the extreme slot orientations, the x axis orientations of radius head are found almost similar. The radius head when the γ equals to 90º is located 0.1mm posteriorly compared to the 0º inclination. The same difference is also observed between the 60º and 30º inclinations. The radius head of model which has 60º inclination is located more posteriorly. However, the radius heads of 30º and 60º inclined slots are oriented more anteriorly compared to the extreme points. Opposite to pronation pose, the main difference in supination obtained along the x axis. From 0º to 90º degree inclination, radius head is shifted more posteriorly within a 9.7mm range. Along z axis, similar to the anterior-posterior shift at the pronation pose, the radius heads of the extreme points oriented at the same location and more medially compared to the mid slot angles. The radius heads of 30º and 60º slots are also oriented at the same location along the z axis and they shifted 1.8mm in lateral direction from the radius heads of the extreme points.

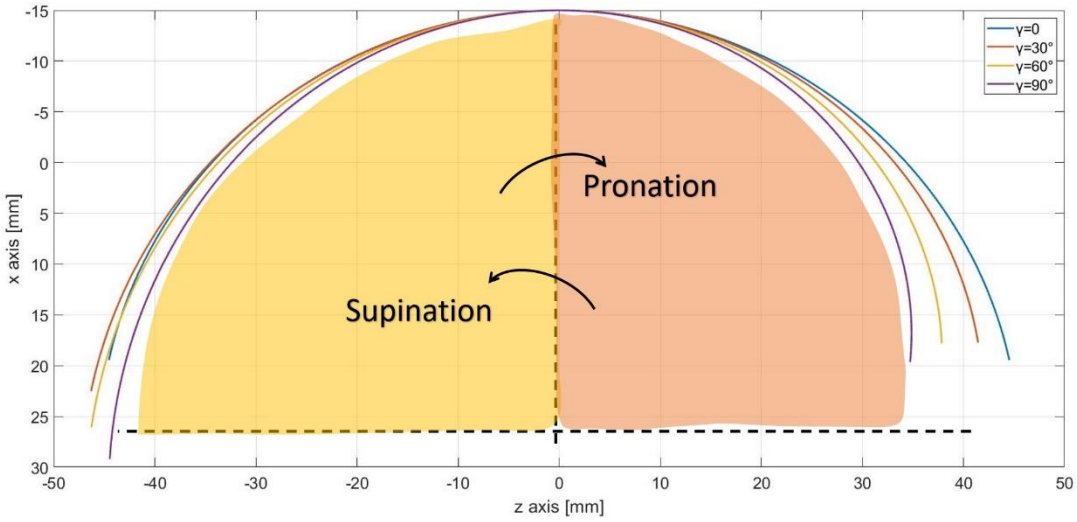

Figure 6.4 The trajectory of radius vector around the MRA on z-x axis for each inclination angle

Table 6.2 Position & range of motion of the distal radius head for each inclination angle of the MRA

	Max Supination			**Max Pronation**		
γ (°)	**Z axis (mm)**	**X axis (mm)**	**Range of motion (°)**	**Z axis (mm)**	**X axis (mm)**	**Range of motion (°)**
0	-44.6	19.5	83.0	44.6	19.5	83.0
30	-46.4	22.6	86.9	41.4	17.7	79.8
60	-46.4	26.2	91.4	37.8	17.8	79.2
90	-44.6	29.3	95.4	34.7	19.6	81.2

Although the main change is observed on the frontal plane during the PS motion, the trajectory of the radius head on the transverse (y-z) and sagittal (y-x) planes have to be analysed as well since the motion of forearm is a complex 3D motion. In Figures 6.5, 6.6, 6.7 and 6.8 the trajectories of the radius head on both planes are shown for each inclination angle in the order of 0, 30º, 60º and 90º. Part (a) and (b) of each Figure show the trajectory on the sagittal and the transverse planes for the specified

inclination angle, respectively. Results show that when the inclination angle is set to be zero, symmetrical radius patterns are observed on both transverse and sagittal planes similar to the frontal plane. However, with the increase in the inclination angle, the asymmetry of the radius pattern increases in both planes. In part (a) and (b) of each Figure anterior-posterior and proximal-distal displacement of the radius head represented. The Figures show that the anterior-posterior and proximal-distal differences between maximum supination and pronation are directly proportional to each other, and both of them increase with 0 to 90º of the inclination angle. Besides, as discussed on the Figure 6.4 and Table 6.2 the main difference in the orientation of the radius head observed in supination phase where the radius head located more posteriorly from 0º to 90º inclination. Furthermore, the results of trajectory on the transverse plane show that increase of the inclination angle enlarges the proximal-distal difference between the maximum supination and pronation from 0 to 2.41mm.

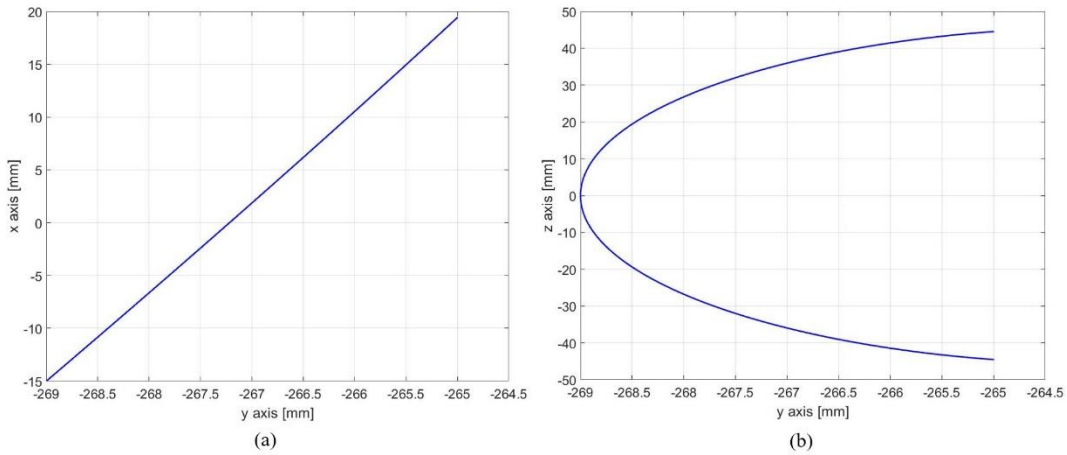

Figure 6.5 Trajectory of the distal head of the radius vector on (a) sagittal and (b) transverse planes when the γ =0

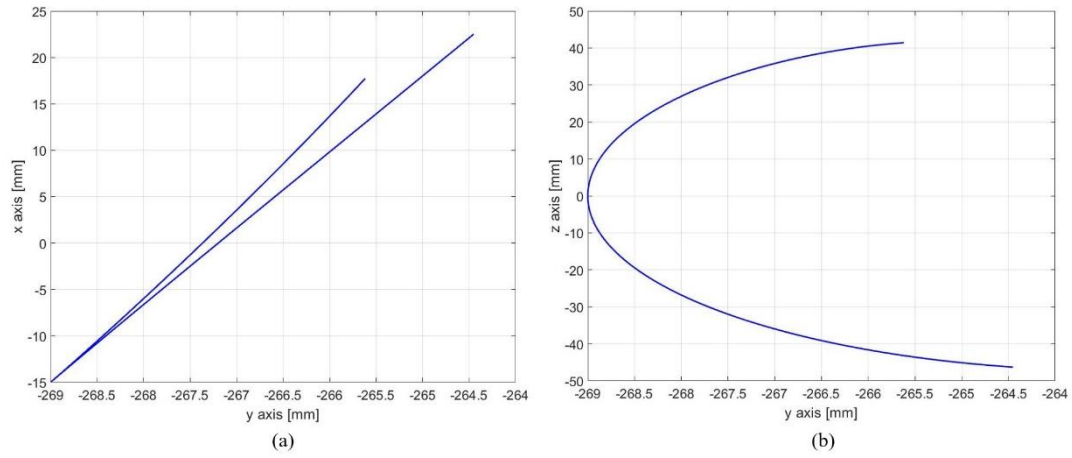

Figure 6.6 Trajectory of the distal head of the radius vector on (a) sagittal and (b) transverse planes when the γ =30º

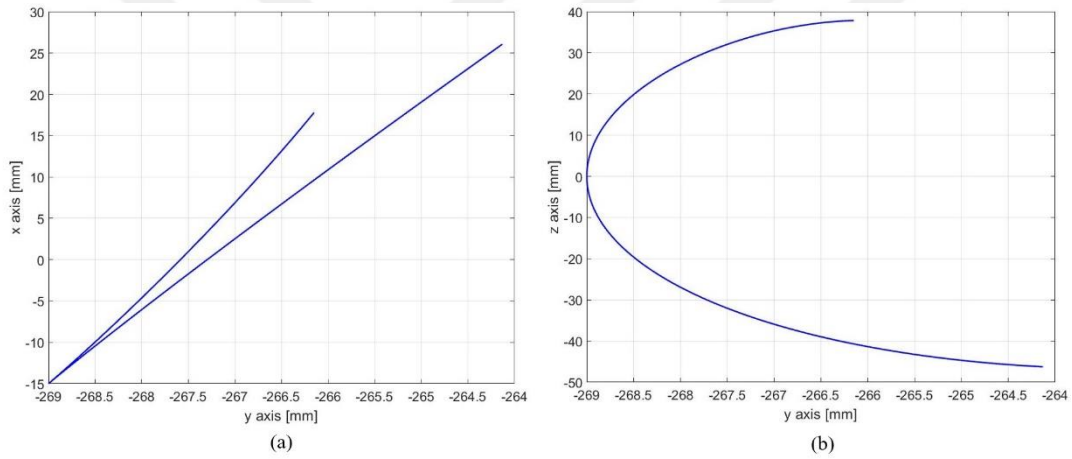

Figure 6.7 Trajectory of the distal head of the radius vector on (a) sagittal and (b) transverse planes when the γ =60º

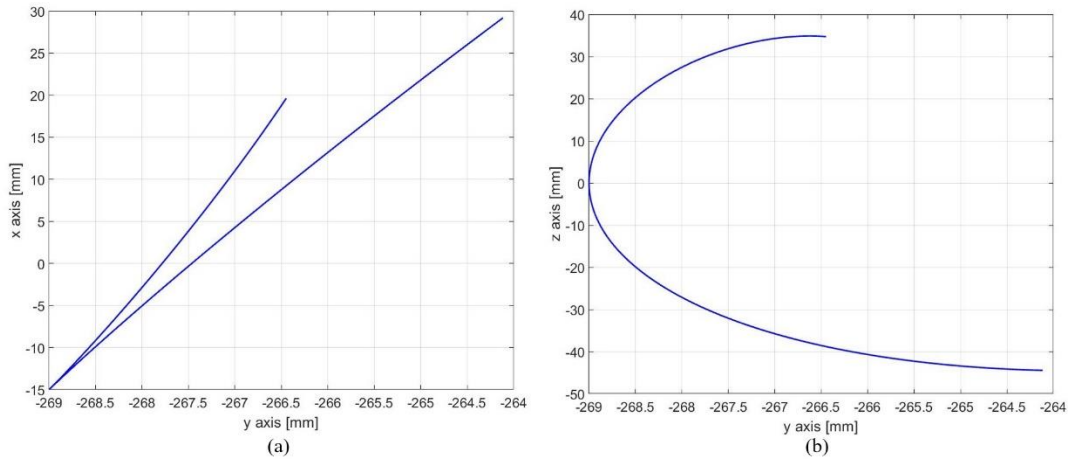

Figure 6.8 Trajectory of the distal head of the radius vector on (a) sagittal and (b) transverse planes when the γ =90º

The results of the different inclination conditions show that from 0 to 90º the motion of the radius head becomes unsymmetric, the total ROM of the radius head increases, and span on the frontal plane is narrowed down 9.8mm (from 89mm to 79.2mm). In the findings of Nakamura et al. (1999), the pattern of the radius head is not purely circular, however, it follows an unsymmetrical pattern that has a shape of near-circular ellipse. When the slot is oriented without an inclination angle, the span is observed its maximum range and the pattern of radius head observed totally symmetrical. The patterns obtained from the 30º, 60º and 90º inclinations are more compatible with the results of Nakamura et al. (1999). For each angle the span is found 88mm, 84.2mm and 79.2mm, respectively. These results show that the radius vectors of the model with higher inclination angles follows more narrowed down patterns, and shapes of the pattern is closer to a near-circular elliptic pattern. Thus, it can be said that 60º and 90º angled inclined slots give more coherent patterns with the literature. Furthermore, when the proximal-distal range obtained from the model is compared with the previous studies, the model results are found quite compatible with the findings of Fischer et al. (2001) (1.4mm translation from maximum supination to pronation) and Fu et al. (2009) (2mm translation from maximum supination to pronation). Besides, the radius head orientation which is found more distally in the supination pose and more proximally in the pronation pose for 30º, 60º

and 90º inclined slots is also compatible with findings of the previous studies for the proximo-distal location of the radius during PS motion (Dumontier & Soubeyrand, 2013; Fischer et al., 2001; Fu et al., 2009; Kapandji, 2007; Tay et al., 2008).

The asymmetry due to slot orientation affects the ROM of pronation and supination poses. It should be noted that, anatomically the pro/supination ROM is measured as the longitudinal rotation of the forearm between the maximum pronation and supination poses. Hence, for the in vivo measurements, the positions of the extremum poses are considered to define the ROM of the forearm rather than the actual amount of rotation around the PS axis. Since the PS axis of forearm arm is not stationary, the rotation amount of the distal radius head will mismatch with the rotation amount about the actual PS axis. In this study, the ROM of the extremum poses are calculated from their orientation which are determined according to the actual PS angles -90º (maximum supination) and 90º (maximum pronation). As it can be seen from the trajectories, with the increase in inclination angle, the radius head location is observed more posterior in supination pose and more anterior in pronation pose which indicates that greater ROM is occurred in supination poses for the 30º, 60º and 90º inclinations. This outcome is also matches with the findings of the previous studies (Akhbari et al., 2021; Fischer et al., 2001; Gattamelata et al., 2007; Rahman et al., 2014; Youm et al., 1979). Although in simple definition the ROMs of supination and pronation are acknowledged as 90º and 85º, respectively, the ROM of each subject differs since the kinematic capability of the bone structure changes from person to person (Gattamelata et al., 2007). The result of the previous studies showed that the average ROMs of supination and pronation can be defined as 82.92º (observed min:48.6º - max:120.78º) and 69.45º (observed min:41.7º - max:106.2º), respectively, and the acceptable range for the total ROM is defined between 152.8º and 185.9º (Akhbari et al., 2021; Fischer et al., 2001; Fu et al., 2009; Gattamelata et al., 2007; Rahman et al., 2014; Wang et al., 2019, 2019; Youm et al., 1979). According to the findings of the previous studies, the total, supination, and pronation ROMs of each inclination angle is obtained within the ranges that previous studies are provided. Besides, the ROM differences between pronation and

supination for 30º, 60º and 90º inclinations are founded compatible with the results of previous studies. However, equal ROMs in both phases when the slot has no inclination, might be observed on few subjects.

To validate the motion characteristics of the proposed model, the MRA model which has 60º inclined slot is compared with the experimental data that is obtained from the whole-body human motion database of the Karlsruher Institut für Technologie (Mandery et al., 2015). After the joint centres are located according to the given algorithm, the PS angle of the forearm is obtained from the homogeneous transformation matrix between the REJC and RWJC. Results presented in Figure 6.9 (a) and (b) show the first and last screw manipulation motions that Subject 912 performs, respectively. The subject rotates his arm from pronation to supination pose for 2 times, and the trajectories of these two motions are compared with the model trajectories within the calculated PS ranges. Within the given frame intervals, results show that the first rotation is started from 90º pronation and performs the supination motion till the 64º supination pose, and last rotation is performed between 81º pronation and 56º supination while the average of the flexion/extension at elbow is found as 75±3.69º. The neutral pose of the forearm is defined according to the motion capture and the PS limits for pronation and supination poses are arrange accordingly. To compare the model results with the motion analysis, the calculated PS ranges of the motion data during the first and last PS rotations of the subject are entered to the model as an input, and the trajectories of the radius vector are calculated to compare its pattern with the experimental measured results. The blue curve shows the trajectory gathered from the motion analysis, where the red and green ones represent the model results with MRA and fixed rotation axis (FRA), respectively. Although the PS motion obtained from the motion data is considered as the forearm rotation around a fixed axis which passes from REJC to RWJC, the results show that the patterns of both models obtained are considerably similar with both screw manipulations. When the plots are compared for the first manipulation, the radius head of the proposed model is oriented lateral and anterior at supination pose and slightly anterior at the pronation pose. Furthermore, during the last manipulation, the

trajectories are observed more consistent compared to first manipulation. At the supination pose the model provide a greater ROM where the opposite is observed for pronation pose.

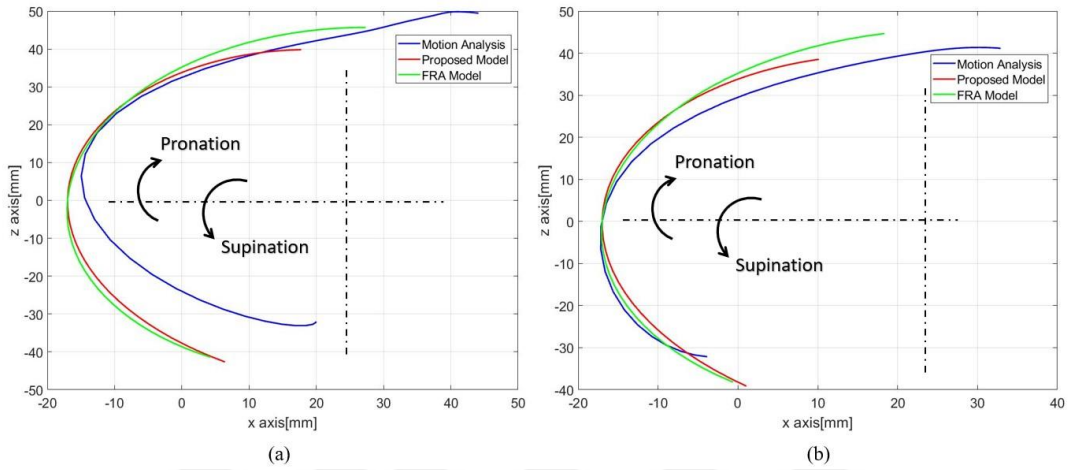

Figure 6.9 Motion analysis vs model results (MRA & FRA); (a) first manipulation (90º :pronation – 64º : supination) (b) last manipulation (81º :pronation – 56º: supination)

The outcomes of inverse and forward kinematics analysis of the model show that results obtained from the inclined slots are more consistent with the literature compared to the case when γ is set to be 0. Since Tay et al. (2010) mentioned that the orientation of the rotation axis pattern differs person to person (Appendix B), the model is tested with different inclinations to observe the change in the motion characteristics of model under the different conditions. Tay et al. (2010) found the patterns in almost linear trend, therefore, the slot of the model is arranged in such a way that the MRA translates on a linear pattern for the simplicity in calculations. Tay et al. (2010) also mentioned that the linear change of the axis represents the gliding amount of radius around the ulna, and including this linear change in a mechanical model might be useful for the modelling of radioulnar joint. The results of the proposed model showed that when the linear change of the rotation axis included as a variable in the model, acceptable trajectories and ROMs can be obtained from the motion of the radial segment. Although the radial motion is found consistent with the literature, the ulnar translation is found less than the findings of

Gattamelata et al. (2007) and Kiyokawa et al. (2015). Gattamelata et al. (2007) mentioned that the amount of ulnar translation might change from person to person according to their anatomical forearm structure, however the pattern shape is expected to be similar for every subject. Thus, further investigations on ulnar translation should be considered together with specific experimentations to improve the motion of ulnar segment.

As mentioned earlier, the main difference of the proposed model compared to the previous models is that the moving rotation axis is included inside the model as a link. In literature, the rotation axis is defined in different ways where some studies fit the forearm rotation on a single titled axis (Hagert, 1992; Hollister et al., 1994a; Oka et al., 2006; Ray et al., 1951; Youm et al., 1979), and more recent studies showed that the axis location changes with the PS motion (Nakamura et al., 1999; Tay et al., 2008, 2010; Veeger et al., 1996). In addition to comparison among the different slot orientations, the model is also tested with the (FRA) and compared with the MRA version to see whether a moving axis is required for modelling, or the same motion can be obtained from the FRA. To turn the proposed model from MRA to FRA, the link of rotation axis is fixed at the midpoint of the MRA slot. Considering the patterns that Tay et al. (2010) defined for 5 different subject, it is assumed that 60º inclined slot might be the closest pattern to the mean of the subjects, and it can give a general understanding on the forearm motion. Therefore, the model version which has 60º slot inclination is chosen for the comparison purposes. The full PS rotation (90º supination to 90º pronation) of the model with 60º inclined slot is given in the Appendix A. Figure 6.10 shows the comparison on the trajectories of radius head when it rotates around the FRA and MRA with 60º inclined slot. From the trajectories it can be seen that the radius head has greater ROM in supination when it rotates around the MRA, and in pronation during the rotation around the FRA. On the other hand, if each trajectory evaluated separately, during the rotation of radius around FRA, greater ROM is observed in pronation pose compared to its supination pose. However, the opposite trend is observed around the MRA. Furthermore, when the

span along the z axis is considered, the trajectory observed around the MRA is more narrowed down compared to the rotation around FRA.

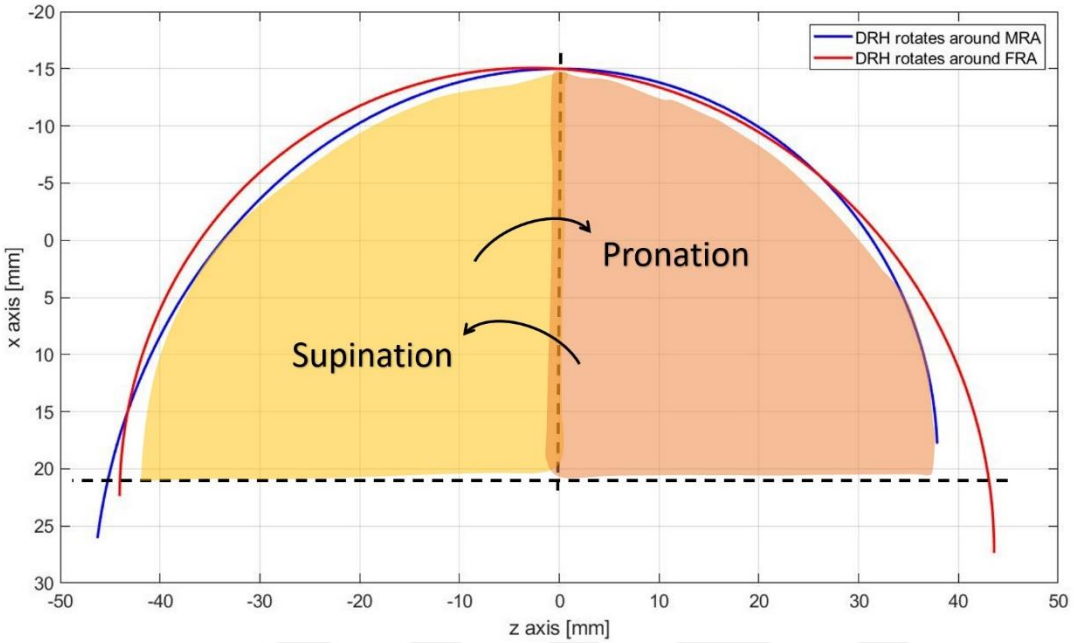

Figure 6.10 FRA vs MRA: Trajectory of the radius head while it is rotating about FRA and MRA (with $\gamma = 60^{o}$)

The comparison in Figure 6.10 shows that the MRA model results are observed more consistent with the findings of the previous studies compared to the FRA model. As it is mentioned by the previous studies, the ROM is greater in supination when the elbow flexed for 90º (Akhbari et al., 2021; Fischer et al., 2001; Gattamelata et al., 2007; Rahman et al., 2014; Youm et al., 1979). However, for the trajectory that obtained from FRA model the opposite is observed. When radius vector is rotated around the FRA, slightly greater pronation pose is observed compared to its supination pose. Although the ROM in pronation pose is less than the maximum pronation pose that Rahman et al. (2014) observed (106.2º), greater pronation pose might rarely happen on subjects since the pronation motion is limited by the ligaments and the bone structure (Soubeyrand et al., 2017). Unlike FRA, when radius vector rotates around the MRA, it preforms grater supination range, and the amount of the ROMs for supination, pronation and total is occurred within ranges that previous studies presented. This comparison shows that including the MRA inside

the model can provide better understanding on the PS motion compared to the FRA, since the results obtained from the MRA are found more consistent with the literature.

The comparisons between the MRA model and the motion analysis data demonstrated at Figure 6.9 (a) and (b) also show that even though the performed pro/supination motion is a subject specific arrangement into the model, the model trajectories are found noticeably close to the radius pattern obtained from the motion analysis. From the trajectories, it can be said that if the model is modified according to the subject specific measurements, more accurate results can be obtained from the comparison. Besides, it should be considered that since the screw manipulation motion requires wrist FE and radioulnar deviation, the uncontrolled wrist motion might affect the marker position at the distal radius head, thus the radius trajectory obtained from the motion data might show some differences with the model results. During the collection of motion data, the Subject 912 performs the screw manipulation with holding a spoon at the air which is not connected to anywhere. Thus, the wrist can freely perform FE and radioulnar deviation. Although the relative motion of the radius is observed from the local frame of the humerus, the wrist motion might affect the location of the RWTS marker. Besides, for the PS angle and the radius trajectory calculations, the rotation axis of the Subject 912's forearm is defined between the REJC and RWJC. This simplification might also affect the trajectory and PS angle. Since the axis is fixed for the motion data, the FRA results are obtained much closer. However, the MRA trajectories are almost same with FRA at the supination. The main difference is observed at the pronation pose. Overall, the results obtained from the proposed model are in an agreement with the outcomes of the previous studies and motion data. Furthermore, the comparison with the motion analysis shows that the proposed model can give more accurate results with the subject specific modifications, and it can provide more realistic understanding on the complex forearm PS motion.

CHAPTER 7

CONCLUSION & FUTURE WORK

For more than a century, many researchers have been working on the forearm motion to understand its complex physiology. However, the knowledge has been gained over years still requires improvements. As the scope of this study, a two-segment novel kinematic forearm model is presented to obtain more realistic forearm motion. Compared to previous kinematic models, the proposed model includes the rotation axis as a link, and the PS rotation is directly defined on a moving rotation axis. Overall, the presented results obtained from the model are founded compatible with the literature. Comparison with the literature shows that among the four inclination angles, 0 inclination angle gives the least consistent results. Although the ROMs of the supination, pronation and total motion of 0 inclination angle case is found within the ranges that previous studies provided, the radius trajectory has to be unsymmetric. On the other hand, for the other inclination angle cases the trajectories of the radius, the ROMs at each phase and the proximo-distal displacement of radius are obtained within the ranges that previous studies mentioned. Furthermore, the ulnar translation trend is found similar to findings of the previous studies, however the amount is found less than what is presented. Therefore, the ulnar motion of the model can be modified according to the further data collection on PS specific task. Moreover, the comparison of MRA and FRA cases shows that the MRA model results are more reliable since the pronation range is observed to be unrealistic for FRA case. Addition to all these analyses, radius trajectories of the model and the experimental data is also compared for the validation of the model. Even though the model is tested without subject specific adjustments, the radius trajectories are considerably similar to each other. This consistency shows that more accurate results can be obtain with the subject specific adjustments. In conclusion, the proposed model yielded consistent trajectories and ROMs when it is compared with the

literature and experimental analysis. Thus, it can be said that by including the rotation axis variation inside the model and defining the PS motion around the moving axis, it is possible to obtain realistic forearm motion.

For further investigations, the model might be tested with a PS specific motion data collection. Since there will be no wrist deviation and elbow flexion, pure PS motion capability of the subject can be investigated. As a possible modification, ulnar sway angle might be included in the model which might improve the orientation of the distal radius head. The other modification might be adding an additional slot at the proximal side of the model. By this modification, more accurate axis orientation can be defined to the model, in other words the radius and hand unit might perform more realistic rotation. However, the model becomes more complex and the proximal radius head must be stabilized to have an anatomically meaningful model. In addition, the effect of the elbow motion on the PS axis might be added into the model. Since it has been found that the PS ranges changes with respect to elbow FE levels (Rahman et al., 2014), this relation can be modelled for obtaining more accurate upper limb modelling.

REFERENCES

Adams, J. E. (2017). Forearm Instability: Anatomy, Biomechanics, and Treatment Options. *The Journal of Hand Surgery*, *42*(1), 47–52. https://doi.org/10.1016/j.jhsa.2016.10.017

Akhbari, B., Shah, K. N., Morton, A. M., Moore, D. C., Weiss, A.-P. C., Wolfe, S. W., & Crisco, J. J. (2021). Biomechanics of the Distal Radioulnar Joint During In Vivo Forearm Pronosupination. *Journal of Wrist Surgery*, *10*(3), 208–215. https://doi.org/10.1055/s-0040-1722334

Alcid, J. G., Ahmad, C. S., & Lee, T. Q. (2004). Elbow anatomy and structural biomechanics. *Clinics in Sports Medicine*, *23*(4), 503–517. https://doi.org/10.1016/j.csm.2004.06.008

Anderson, RichardJ. (1901). ROTATION OF THE FOREARM. *The Lancet*, *158*(4081), 1333–1334. https://doi.org/10.1016/S0140-6736(01)73986-4

Birkbeck, D. P., Failla, J. M., Hoshaw, S. J., Fyhrie, D. P., & Schaffler, M. (1997). The interosseous membrane affects load distribution in the forearm. *The Journal of Hand Surgery*, *22*(6), 975–980. https://doi.org/10.1016/S0363-5023(97)80035-4

Capener, N. (1956). THE HAND IN SURGERY. *The Journal of Bone and Joint Surgery. British Volume*, *38-B*(1), 128–151. https://doi.org/10.1302/0301-620X.38B1.128

Chao, E. Y., & Morrey, B. F. (1978). Three-dimensional rotation of the elbow. *Journal of Biomechanics*, *11*(1–2), 57–73. https://doi.org/10.1016/0021-9290(78)90044-1

Chen, Y., Li, G., Zhu, Y., Zhao, J., & Cai, H. (2014). Design of a 6-DOF upper limb rehabilitation exoskeleton with parallel actuated joints. *Bio-Medical Materials and Engineering*, *24*(6), 2527–2535. https://doi.org/10.3233/BME-141067

Chidgey, L. K. (1995). The Distal Radioulnar Joint:Problems and Solutions. *JAAOS - Journal of the American Academy of Orthopaedic Surgeons*, *3*(2), 95–109.

Christensen, J. B., Adams, J. P., Cho, K. O., & Miller, L. (1968). A study of the interosseous distance between the radius and ulna during rotation of the forearm. *The Anatomical Record*, *160*(2), 261–271. https://doi.org/10.1002/ar.1091600212

Doyle, J. R., & Botte, M. J. (2003). *Surgical anatomy of the hand and upper extremity*. Lippincott Williams & Wilkins.

Dumontier, C., & Soubeyrand, M. (2013). The Forearm Joint. In G. Bentley (Ed.), *European Instructional Lectures* (pp. 181–194). Springer Berlin Heidelberg. https://doi.org/10.1007/978-3-642-36149-4_14

Duprey, S., Naaim, A., Moissenet, F., Begon, M., & Chèze, L. (2017). Kinematic models of the upper limb joints for multibody kinematics optimisation: An overview. *Journal of Biomechanics*, *62*, 87–94. https://doi.org/10.1016/j.jbiomech.2016.12.005

Dwight, T. (1885). The Movements of the Ulna in Rotation of the Fore-Arm. *Journal of Anatomy and Physiology*, *19*(Pt 2), 186–189.

Fischer, K. J., Manson, T. T., Pfaeffle, H. J., Tomaino, M. M., & Woo, S. L.-Y. (2001). A method for measuring joint kinematics designed for accurate

registration of kinematic data to models constructed from CT data. *Journal of Biomechanics*, *34*(3), 377–383. https://doi.org/10.1016/S0021-9290(00)00195-0

Fohanno, V., Begon, M., Lacouture, P., & Colloud, F. (2014). Estimating joint kinematics of a whole body chain model with closed-loop constraints. *Multibody System Dynamics*, *31*(4), 433–449. https://doi.org/10.1007/s11044-013-9366-7

Fohanno, V., Lacouture, P., & Colloud, F. (2013). Improvement of upper extremity kinematics estimation using a subject-specific forearm model implemented in a kinematic chain. *Journal of Biomechanics*, *46*(6), 1053–1059. https://doi.org/10.1016/j.jbiomech.2013.01.029

Fu, E., Li, G., Souer, J. S., Lozano-Calderon, S., Herndon, J. H., Jupiter, J. B., & Chen, N. C. (2009). Elbow Position Affects Distal Radioulnar Joint Kinematics. *The Journal of Hand Surgery*, *34*(7), 1261–1268. https://doi.org/10.1016/j.jhsa.2009.04.025

Gattamelata, D., Pezzuti, E., & Valentini, P. P. (2007). Accurate geometrical constraints for the computer aided modelling of the human upper limb. *Computer-Aided Design*, *39*(7), 540–547. https://doi.org/10.1016/j.cad.2007.01.009

Green, J. B., & Zelouf, D. S. (2009). Forearm Instability. *The Journal of Hand Surgery*, *34*(5), 953–961. https://doi.org/10.1016/j.jhsa.2009.03.018

Guo, S., Zhang, W., Wei, W., Guo, J., Ji, Y., & Wang, Y. (2013). A kinematic model of an upper limb rehabilitation robot system. *2013 IEEE International*

Conference on Mechatronics and Automation, 968–973. https://doi.org/10.1109/ICMA.2013.6618046

Hagert, C. (1992). The distal radioulnar joint in relation to the whole forearm. *Clinical Orthopaedics and Related Research*, *275*, 56–64.

Hagert, C.-G. (1992). The Distal Radioulnar Joint in Relation to the Whole Forearm. *Clinical Orthopaedics and Related Research (1976-2007)*, *275*, 56.

Heiberg, J. (1885). Movements of the Ulna in Rotation of the Fore-Arm. *Journal of Anatomy and Physiology*, *19*(Pt 3), 237–240.

Hollister, A. M., Gellman, H., & Waters, R. L. (1994a). The Relationship of the Interosseous Membrane to the Axis of Rotation of the Forearm. *Clinical Orthopaedics and Related Research (1976-2007)*, *298*, 272.

Hollister, A. M., Gellman, M. H., & Waters, R. L. (1994b). The relationship of the interossesous membrance to the axis of rotation of the forearm. *Clinical Orthopaedics and Related Research*, *298*, 272–276.

Huang, J. I., & Hanel, D. P. (2012). Anatomy and Biomechanics of the Distal Radioulnar Joint. *Hand Clinics*, *28*(2), 157–163. https://doi.org/10.1016/j.hcl.2012.03.002

Kapandji, I. A. (2007). *The physiology of the joints* (6th ed., English ed). Churchill Livingstone.

Kecskeméthy, A., & Weinberg, A. (2005). An Improved Elasto-Kinematic Model of the Human Forearm for Biofidelic Medical Diagnosis. *Multibody System Dynamics*, *14*(1), 1–21. https://doi.org/10.1007/s11044-005-1756-z

Kiyokawa, T., Nojiri, K., Ohtsuka, H., & Okayama, Y. (2015). Estimation of kinematics parameters dependent on pronation supination for modeling forearm skeletal system based on CT images. *2015 IEEE/SICE International Symposium on System Integration (SII)*, 422–427. https://doi.org/10.1109/SII.2015.7405016

Kontaxis, A., Cutti, A. G., Johnson, G. R., & Veeger, H. E. J. (2009). A framework for the definition of standardized protocols for measuring upper-extremity kinematics. *Clinical Biomechanics*, *24*(3), 246–253. https://doi.org/10.1016/j.clinbiomech.2008.12.009

Laitenberger, M., Raison, M., Périé, D., & Begon, M. (2015). Refinement of the upper limb joint kinematics and dynamics using a subject-specific closed-loop forearm model. *Multibody System Dynamics*, *33*(4), 413–438. https://doi.org/10.1007/s11044-014-9421-z

LaStayo, P. C., & Lee, M. J. (2006). The Forearm Complex: Anatomy, Biomechanics and Clinical Considerations. *Journal of Hand Therapy*, *19*(2), 137–145. https://doi.org/10.1197/j.jht.2006.02.002

Lemay, M. A., & Crago, P. E. (1996). A dynamic model for simulating movements of the elbow, forearm, and wrist. *Journal of Biomechanics*, *29*(10), 1319–1330. https://doi.org/10.1016/0021-9290(96)00026-7

Mandery, C., Terlemez, Ö., Do, M., Vahrenkamp, N., & Asfour, T. (2015). *The KIT Whole-Body Human Motion Database*. 329–336.

Markolf, K. L., Dunbar, A. M., & Hannani, K. (2000). Mechanisms of load transfer in the cadaver forearm: Role of the interosseous membrane. *The Journal of Hand Surgery*, *25*(4), 674–682. https://doi.org/10.1053/jhsu.2000.8640

Matsuki, K. O., Matsuki, K., Mu, S., Sasho, T., Nakagawa, K., Ochiai, N., Takahashi, K., & Banks, S. A. (2010). In vivo 3D kinematics of normal forearms: Analysis of dynamic forearm rotation. *Clinical Biomechanics*, *25*(10), 979–983. https://doi.org/10.1016/j.clinbiomech.2010.07.006

Matthews, L. S., Kaufer, H., Garver, D. F., & Sonstegard, D. A. (1982). The effect on supination-pronation of angular malalignment of fractures of both bones of the forearm.: *The Journal of Bone & Joint Surgery*, *64*(1), 14–17. https://doi.org/10.2106/00004623-198264010-00003

McGinley, J. C., & Kozin, S. H. (2001). Interosseous Membrane Anatomy and Functional Mechanics. *Clinical Orthopaedics and Related Research®*, *383*, 108–122.

Morrey, B. F., Sanchez-Sotelo, J., & Morrey, M. E. (Eds.). (2018). *Morrey's the elbow and its disorders* (Fifth edition). Elsevier.

Nakamura, T., Yabe, Y., Horiuchi, Y., & Yamazaki, N. (1999). In vivo motion analysis of forearm rotation utilizing magnetic resonance imaging. *Clinical Biomechanics*, *14*(5), 315–320. https://doi.org/10.1016/S0268-0033(98)90091-2

Nojiri, K., Matsunaga, N., & Kawaji, S. (2006). Inverse Dynamics Analysis of Forearm in CPM. *2006 SICE-ICASE International Joint Conference*, 2336–2339. https://doi.org/10.1109/SICE.2006.315498

Oka, K., Doi, K., Suzuki, K., Murase, T., Goto, A., Yoshikawa, H., Sugamoto, K., & Moritomo, H. (2006). In vivo three-dimensional motion analysis of the forearm with radioulnar synostosis treated by the kanaya procedure. *Journal of Orthopaedic Research*, *24*(5), 1028–1035. https://doi.org/10.1002/jor.20136

Özgören, M. K. (2019). *Kinematics of general spatial mechanical systems*. Wiley.

Palmer, A. K., Glisson, R. R., & Werner, F. W. (1982). Ulnar variance determination. *The Journal of Hand Surgery*, *7*(4), 376–379. https://doi.org/10.1016/S0363-5023(82)80147-0

Palmer, A. K., Werner, F. W., Murphy, D., & Glisson, R. (1985). Functional wrist motion: A biomechanical study. *The Journal of Hand Surgery*, *10*(1), 39–46. https://doi.org/10.1016/S0363-5023(85)80246-X

Palmer, A., & Werner, F. (1984). Biomechanics of the distal radioulnar joint. *Clinical Orthopaedics and Related Research*. https://doi.org/10.1097/00003086-198407000-00005

Pennestrì, E., Stefanelli, R., Valentini, P. P., & Vita, L. (2007). Virtual musculo-skeletal model for the biomechanical analysis of the upper limb. *Journal of Biomechanics*, *40*(6), 1350–1361. https://doi.org/10.1016/j.jbiomech.2006.05.013

Prokopenko, R. A., Frolov, A. A., Biryukova, E. V., & Roby-Brami, A. (2001). Assessment of the accuracy of a human arm model with seven degrees of freedom. *Journal of Biomechanics*, *34*(2), 177–185. https://doi.org/10.1016/S0021-9290(00)00179-2

Rabinowitz, R. S., Light, T. R., Havey, R. M., Gourineni, P., Patwardhan, A. G., Sartori, M. J., & Vrbos, L. (1994). The role of the interosseous membrane and triangular fibrocartilage complex in forearm stability. *The Journal of Hand Surgery*, *19*(3), 385–393. https://doi.org/10.1016/0363-5023(94)90050-7

Rahman, H. A., Fai, Y. C., & Ming, E. S. L. (2014). Analysis of Human Hand Kinematics: Forearm Pronation and Supination. *Journal of Medical Imaging and Health Informatics*, *4*(2), 245–249. https://doi.org/10.1166/jmihi.2014.1239

Raikova, R. (1992). A general approach for modelling and mathematical investigation of the human upper limb. *Journal of Biomechanics*, *25*(8), 857–867. https://doi.org/10.1016/0021-9290(92)90226-Q

Ramananarivo, M., Raison, M., Barron, O., & Achiche, S. (2017). Biofidelic design of the forearm of a myoelectric prosthesis with maximum functional volume. *DS 87-1 Proceedings of the 21st International Conference on Engineering Design (ICED 17) Vol 1: Resource Sensitive Design, Design Research Applications and Case Studies, Vancouver, Canada, 21-25.08.2017*, 479–488.

Ray, R. D., Johnson, R. J., & Jameson, R. M. (1951). ROTATION OF THE FOREARM: An Experimental Study of Pronation and Supination. *JBJS*, *33*(4), 993–996.

Robbin, M. L., An, K. N., Linscheid, R. L., & Ritman, E. L. (1986). Anatomic and kinematic analysis of the human forearm using high-speed computed

tomography. *Medical and Biological Engineering and Computing, 24*(2), 164–168. https://doi.org/10.1007/BF02443930

Rose-Innes, A. P. (1960). Anterior dislocation of the ulna at the inferior radio-ulnar joint: Case reports, with a discussion of the anatomy of rotation of the forearm. *The Journal of Bone and Joint Surgery. British Volume, 42*(3), 515–521.

Soubeyrand, M., Assabah, B., Bégin, M., Laemmel, E., Dos Santos, A., & Crézé, M. (2017). Pronation and supination of the hand: Anatomy and biomechanics. *Hand Surgery and Rehabilitation*, *36*(1), 2–11. https://doi.org/10.1016/j.hansur.2016.09.012

Tay, S. C., van Riet, R., Kazunari, T., Amrami, K. K., An, K.-N., & Berger, R. A. (2010). In-vivo kinematic analysis of forearm rotation using helical axis analysis. *Clinical Biomechanics*, *25*(7), 655–659. https://doi.org/10.1016/j.clinbiomech.2010.03.010

Tay, S. C., van Riet, R., Kazunari, T., Koff, M. F., Amrami, K. K., An, K.-N., & Berger, R. A. (2008). A method for in-vivo kinematic analysis of the forearm. *Journal of Biomechanics*, *41*(1), 56–62. https://doi.org/10.1016/j.jbiomech.2007.07.019

Tsai, P. C., & Paksima, N. (2009). The distal radioulnar joint. *Bulletin of the NYU Hospital for Joint Diseases*, *67*(1), 90.

van Andel, C. J., Wolterbeek, N., Doorenbosch, C. A. M., Veeger, D. (H. E. J.), & Harlaar, J. (2008). Complete 3D kinematics of upper extremity functional

tasks. *Gait & Posture*, *27*(1), 120–127. https://doi.org/10.1016/j.gaitpost.2007.03.002

Van Sint Jan, S., Salvia, P., Hilal, I., Sholukha, V., Rooze, M., & Clapworthy, G. (2002). Registration of 6-DOFs electrogoniometry and CT medical imaging for 3D joint modeling. *Journal of Biomechanics*, *35*(11), 1475–1484. https://doi.org/10.1016/S0021-9290(02)00074-X

Veeger, H. E. J., & Yu, B. (1996). Orientation of axes in the elbow and forearm for biomechanical modelling. *Proceedings of the 1996 Fifteenth Southern Biomedical Engineering Conference*, 377–380. https://doi.org/10.1109/SBEC.1996.493254

Veeger, H. E. J., Yu, B., & An, K. N. (1996). Orientation of axes in the elbow and forearm for biomechanical modeling. *Proceedings of the First Conference of the International Shoulder Group. Shaker Publishing, Maastricht*, 83–87.

Vicon Motion Systems. (2010). *Plug-in-Gait Marker Placement*.

Wang, W., Wang, D., Wesseling, M., Xue, B., & Li, F. (2019). Comparison of modelling and tracking methods for analysing elbow and forearm kinematics. *Proceedings of the Institution of Mechanical Engineers, Part H: Journal of Engineering in Medicine*, *233*(11), 1113–1121. https://doi.org/10.1177/0954411919872400

Weinberg, A. M., Pietsch, I. T., Helm, M. B., Hesselbach, J., & Tscherne, H. (2000). A new kinematic model of pro- and supination of the human forearm. *Journal of Biomechanics*, *33*(4), 487–491. https://doi.org/10.1016/S0021-9290(99)00195-5

Weiss, A.-P. C., & Hastings, H. (1992). The anatomy of the proximal radioulnar joint. *Journal of Shoulder and Elbow Surgery*, *1*(4), 193–199. https://doi.org/10.1016/1058-2746(92)90013-S

Yoon, D., Lee, G., & Choi, Y. (2019). Kinematic Modeling of Distal Radioulnar Joint for Human Forearm Rotation. *The Journal of Korea Robotics Society*, *14*(4), 251–257. https://doi.org/10.7746/jkros.2019.14.4.251

Youm, Y., Dryer, R. F., Thambyrajah, K., Flatt, A. E., & Sprague, B. L. (1979). Biomechanical analyses of forearm pronation-supination and elbow flexion-extension. *Journal of Biomechanics*, *12*(4), 245–255. https://doi.org/10.1016/0021-9290(79)90067-8

Zampagni, M. L., Casino, D., Martelli, S., Visani, A., & Marcacci, M. (2008). A protocol for clinical evaluation of the carrying angle of the elbow by anatomic landmarks. *Journal of Shoulder and Elbow Surgery*, *17*(1), 106–112. https://doi.org/10.1016/j.jse.2007.03.028

Zimmerman, N. B. (2002). Clinical application of advances in elbow and forearm anatomy and biomechanics. *Hand Clinics*, *18*(1), 1–19. https://doi.org/10.1016/S0749-0712(02)00010-0

APPENDICES

A. 3D Motion of the Radius Segment of the Model

Figure A.1 shows the 3D motion of the proposed model when the slot is located with the 60º inclination angle, γ. The orientation of the radius segment at 11 different PS poses are represented in the figure. Red and blue coloured lines are used to represent the link the radius and MRA links, respectively. The colour of the radius segment plane changes from darker to lighter when the radius segment moves from its natural pose to maximum supination and maximum pronation. Among the 11 data points, the maximum supination, neutral and maximum pronation poses are shown with red, green, and blue dots.

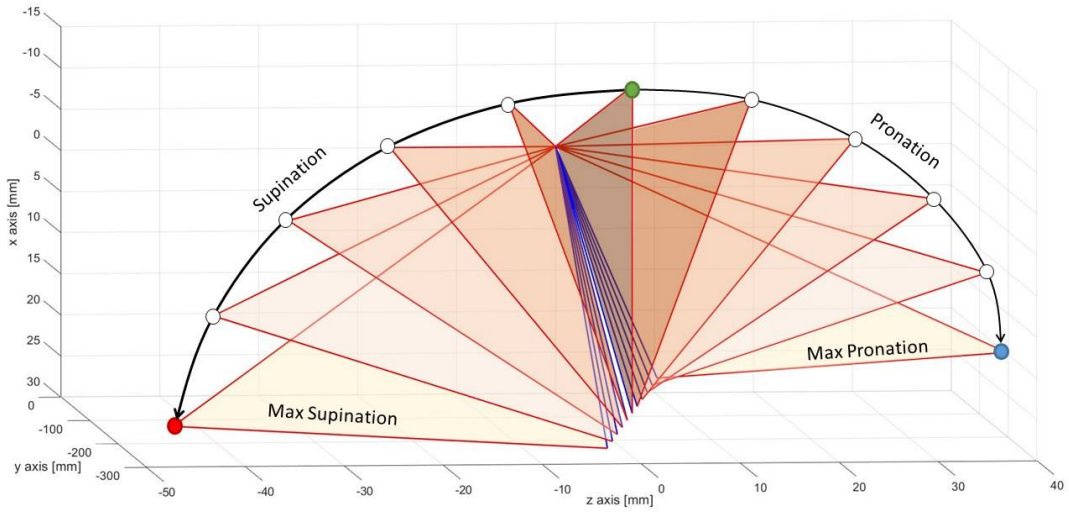

Figure A.1 3D Motion of the Radius Segment of the Model when the γ =60º

B. Rotation Axis Patterns for Different Subjects & Sample MRA Pattern

Figure A.2(a) shows the patterns of the rotation axis at the distal end for different subjects according to the Tay et al. (2010)'s findings and Figure A.2(b) shows the slot orientation of 60º inclined slot on the distal end. As it can be seen that for each subject the rotation axis varies in different patterns, however they follow almost linear paths. In the test of the model, it is assumed that among the 4 tested inclination angles 60º inclined slot might give better understanding of the motion characteristics of an average subject.

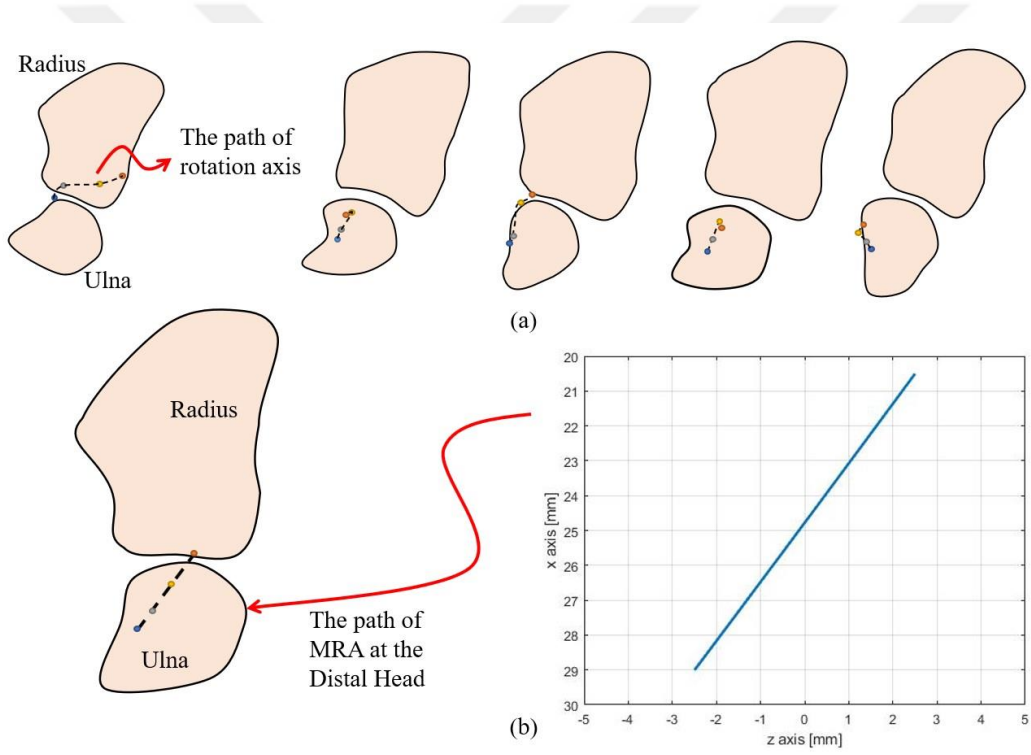

Figure A.2 (a) Different rotation axis patterns for different Subjects (b) MRA pattern when the $\gamma = 60^{o}$

C. Derivation of the Joint Variables

From the solution of Equation 7 & 8

$$\begin{bmatrix} 1 & 0 & 0 & r_1 - r_3 s_2 \sin\gamma \\ 0 & 1 & 0 & -r_2 + s_1 \\ 0 & 0 & 1 & s_2 \cos\gamma \\ 0 & 0 & 0 & 1 \end{bmatrix} = \begin{bmatrix} C_{11} & C_{12} & C_{13} & r_4 \cos\phi_2 \sin\phi_1 \\ C_{21} & C_{22} & C_{23} & -r_4 \cos\phi_2 \cos\phi_1 \\ C_{31} & C_{32} & C_{33} & -r_4 \sin\phi_2 \\ 0 & 0 & 0 & 1 \end{bmatrix}$$

In the equations down below "c" stands for cosine and "s" stands for sine.

$$C_{11} = \mathrm{c}\,\psi_1\,\mathrm{c}\,\phi_1 - \mathrm{s}\,\psi_1\,(\mathrm{c}\,\psi_2\,\mathrm{c}\,\phi_2\,\mathrm{s}\,\phi_1 - \mathrm{s}\,\phi_1\,\mathrm{s}\,\psi_2\,\mathrm{s}\,\phi_2)$$

$$C_{12} = -\,\mathrm{c}\,\psi_1\,(\mathrm{c}\,\psi_2\,\mathrm{c}\,\phi_2\,\mathrm{s}\,\phi_1 - \mathrm{s}\,\phi_1\,\mathrm{s}\,\psi_2\,\mathrm{s}\,\phi_2) - \mathrm{c}\,\phi_1\,\mathrm{s}\,\psi_1$$

$$C_{13} = \mathrm{c}\,\psi_2\,\mathrm{s}\,\phi_2\,\mathrm{s}\,\phi_1 + \mathrm{s}\,\phi_1\,\mathrm{s}\,\psi_2\,\mathrm{c}\,\phi_2$$

$$C_{21} = \mathrm{s}\,\psi_1\,(\mathrm{c}\,\psi_2\,\mathrm{c}\,\phi_2\,\mathrm{c}\,\phi_1 - \mathrm{c}\,\phi_1\,\mathrm{s}\,\psi_2\,\mathrm{s}\,\phi_2) + \mathrm{s}\,\phi_1\,\mathrm{c}\,\psi_1$$

$$C_{22} = \mathrm{c}\,\psi_1\,(\mathrm{c}\,\psi_2\,\mathrm{c}\,\phi_2\,\mathrm{c}\,\phi_1 - \mathrm{c}\,\phi_1\,\mathrm{s}\,\psi_2\,\mathrm{s}\,\phi_2) - \mathrm{s}\,\phi_1\,\mathrm{s}\,\psi_1$$

$$C_{23} = -\,\mathrm{c}\,\psi_2\,\mathrm{c}\,\phi_1\,\mathrm{s}\,\phi_2 - \mathrm{s}\,\psi_2\,\mathrm{c}\,\phi_1\,\mathrm{c}\,\phi_2$$

$$C_{31} = \mathrm{s}\,\psi_1\,(\mathrm{c}\,\psi_2\,\mathrm{s}\,\phi_2 + \mathrm{s}\,\psi_2\,\mathrm{c}\,\phi_2)$$

$$C_{32} = \mathrm{c}\,\psi_1\,(\mathrm{c}\,\psi_2\,\mathrm{s}\,\phi_2 + \mathrm{s}\,\psi_2\,\mathrm{c}\,\phi_2)$$

$$C_{33} = \mathrm{c}\,\psi_2\,\mathrm{c}\,\phi_2 - \mathrm{s}\,\psi_2\,\mathrm{s}\,\phi_2$$

The joint variables are defined accordingly.

To find the ϕ_2:

$$-r_4 \sin\phi_2 = s_2 \cos\gamma$$

$$\sin\phi_2 = \frac{s_2 \cos\gamma}{-r_4}$$

$$\sin^2\phi_2 + \cos^2\phi_2 = 1$$

$$\cos\phi_2 = \sigma_1 \frac{\sqrt{{r_4}^2 - {s_2}^2\cos^2\gamma}}{r_4}$$

$$\boldsymbol{\phi_2 = atan_2\left(\frac{-s_2\cos\gamma}{r_4}, \sigma_1\frac{\sqrt{{r_4}^2 - {s_2}^2\cos^2\gamma}}{r_4}\right), \sigma_1 = +1}$$

To find the s_1:

$$Take\ the\ square\ of\ both\ and\ add \begin{cases} -r_2 + s_1 = -r_4\cos\phi_2\cos\phi_1 \\ r_1 - r_3 - s_2\sin\gamma = r_4\cos\phi_2\sin\phi_1 \end{cases}$$

$$(-r_2 + s_1)^2 + (r_1 - r_3 - s_2\sin\gamma)^2 = {r_4}^2\cos^2\phi_2$$

$$\boldsymbol{s_1 = r_2 + \sigma_2\sqrt{{r_4}^2\cos^2\emptyset_2 - (r_1 - r_3 - s_2\sin\gamma)^2};\ \sigma_2 = -1}$$

To find the ϕ_1:

$$-r_2 + s_1 = -r_4\cos\phi_2\cos\phi_1$$

$$\cos\phi_1 = \frac{-r_2 + s_1}{-r_4\cos\phi_2}$$

$$r_1 - r_3 - s_2\sin\gamma = r_4\cos\phi_2\sin\phi_1$$

$$\sin\phi_1 = \frac{r_1 - r_3 - s_2\sin\gamma}{r_4\cos\phi_2}$$

$$\boldsymbol{\phi_1 = atan_2\left(\frac{r_1 - r_3 - s_2\sin\gamma}{r_4\cos\phi_2}, \frac{-r_2 + s_1}{-r_4\cos\phi_2}\right)}$$

To find the ψ_1 & ψ_2:

$$C_{33} = \mathrm{c}\,\psi_2\,\mathrm{c}\,\phi_2 - \mathrm{s}\,\psi_2\,\mathrm{s}\,\phi_2 = 1$$

$$\mathrm{c}\,\psi_2\,\mathrm{c}\,\phi_2 - \mathrm{s}\,\psi_2\,\mathrm{s}\,\phi_2 = c(\psi_2 + \phi_2) = 1$$

$$\psi_2 + \phi_2 = 0;\ \Longrightarrow\ \boldsymbol{\psi_2 = -\phi_2}$$

$$C_{22} = \mathrm{c}\,\psi_1\,(\mathrm{c}\,\psi_2\,\mathrm{c}\,\phi_2\,\mathrm{c}\,\phi_1 - \mathrm{c}\,\phi_1\,\mathrm{s}\,\psi_2\,\mathrm{s}\,\phi_2) - \mathrm{s}\,\phi_1\,\mathrm{s}\,\psi_1 = 1$$

$$\mathrm{c}\,\psi_1\,(\mathrm{c}\,\psi_2\,\mathrm{c}\,\phi_2\,\mathrm{c}\,\phi_1 - \mathrm{c}\,\phi_1\,\mathrm{s}\,\psi_2\,\mathrm{s}\,\phi_2) - \mathrm{s}\,\phi_1\,\mathrm{s}\,\psi_1$$
$$= \mathrm{c}\,\psi_1\,\mathrm{c}\,\phi_1\,(\mathrm{c}\,\psi_2\,\mathrm{c}\,\phi_2 - \mathrm{s}\,\psi_2\,\mathrm{s}\,\phi_2) - \mathrm{s}\,\phi_1\,\mathrm{s}\,\psi_1$$

$;where\ \mathrm{c}\,\psi_2\,\mathrm{c}\,\phi_2 - \mathrm{s}\,\psi_2\,\mathrm{s}\,\phi_2 = 1$

$$\mathrm{c}\,\psi_1\,\mathrm{c}\,\phi_1 - \mathrm{s}\,\phi_1\,\mathrm{s}\,\psi_1 = c(\psi_1 + \phi_1) = 1$$

$$\psi_1 + \phi_1 = 0; \implies \boldsymbol{\psi_1 = -\phi_1}$$